FINITE ELEMENT MODEL UPDATING USING ANTIRESONANT FREQUENCIES

THESIS

Keith W. Jones, First Lieutenant, USAF

AFIT/GAE/ENY/00M-08

20000803 144

DEPARTMENT OF THE AIR FORCE

AIR UNIVERSITY

AIR FORCE INSTITUTE OF TECHNOLOGY

Wright-Patterson Air Force Base, Ohio

APPROVED FOR PUBLIC RELEASE; DISTRIBUTION UNLIMITED.

DTIC QUALITY INSPECTED 4

AFIT/GAE/ENY/00M-08

FINITE ELEMENT MODEL UPDATING USING ANTIRESONANT FREQUENCIES

THESIS

Presented to the Faculty

Department of Aeronautical Engineering

Graduate School of Engineering and Management

Air Force Institute of Technology

Air University

Air Education and Training Command

In Partial Fulfillment of the Requirements for the

Degree of Master of Science in Aeronautical Engineering

Keith W. Jones, B.S.
First Lieutenant, USAF

March 2000

APPROVED FOR PUBLIC RELEASE; DISTRIBUTION UNLIMITED.

AFIT/GAE/ENY/00M-08

FINITE ELEMENT MODEL UPDATING USING ANTIRESONANT FREQUENCIES

Keith W. Jones, B.S.

First Lieutenant, USAF

Approved:

LtCol Jeffrey Turcotte Committee Chairman	07 MAR 2000 Date
Dr. Bradley Liebst Committee Member	07 MAR 00 Date
Capt Gregory Agnes Committee Member	9 Mar 00 Date

Acknowledgments

I would like to recognize several people who played important roles in this research. Thank you Lieutenant Colonel Turcotte for your excellent teaching and guidance in and out of class. The time spent in your office discussing this project and your time spent in the laboratory troubleshooting problems was greatly appreciated. Thanks also to Lt. Doug Gaeta for collecting and sharing your data with me. Special thanks also go to Capt. Eric Swenson who was kind enough to travel back to AFIT and share his model updating and damage detection expertise as well as provide electronic copies of pictures and figures so that they would not have to be redone. I am also very grateful to Mr. Jay Anderson for his timely support in acquiring the software and laboratory equipment needed.

Most of all, I want to thank God for providing me motivation and understanding in answer to my prayers. To my gracious wife Claudia, who loved and supported me throughout this process, I express my deepest admiration and love.

Table Of Contents

Page

Acknowledgments iv

Table Of Contents v

List of Figures viii

List of Tables ix

List of Symbols x

List of Abbreviations xiv

Abstract xv

Chapter 1. INTRODUCTION 1

1.1 Finite Element Model Updating 1

1.2 Problems with Modal Updating Methods 3

1.3 Antiresonance 4

1.4 Thesis Objective 5

1.5 Thesis Overview 5

Chapter 2. BACKGROUND 6

2.1 Finite Element Model Updating 6

2.2 Damage Detection 7

2.3 Antiresonance 8

2.4 Previous Research on the Flexible Truss Experiment 11

2.5 Joint Modeling 13

2.6 Summary 19

Chapter 3. THEORY 20

3.1 Antiresonance / Mode Shape Relationship 20

3.2 Calculating Antiresonant Frequencies 22

3.3 Model Updating - Penalty Method 23

3.4 Penalty Method Extended to Include Antiresonant Frequencies 25

3.5 Eigenvalue Sensitivities 26

3.6 Antiresonance Sensitivities 26

3.7 Mode Pairing 28

Chapter 4. EXPERIMENTAL SETUP 30

4.1 Flexible Truss Experiment 30

4.2 Actuators and Sensors 32

4.3 Data Collection 33

Chapter 5. FINITE ELEMENT MODELING 34

5.1 Finite Element Method 34

5.2 Finite Elements Used 35

5.3 Non-Linear Stress Softening 36

5.4 Joint Model 38

5.5 Initial Model Results 40

Chapter 6. FINITE ELEMENT MODEL UPDATING 44

6.1 Introduction 44

6.2 Overview 44

6.3 Eigenvalue and Antiresonance Identification 47

6.4 Choice of Update Parameters 48

6.5 Choice of Weighting Matrices 50

6.6 Updating Results 51

Chapter 7. DAMAGE DETECTION 56

7.1 Introduction 56

7.2 Flexible Truss Experiment Damage 56

7.3 Pattern Classification Method 58

7.4 Curve-Fit Method 59

7.5 Damage Detection Results - 32 Damage Cases 60

7.6 Damage Detection Results - 112 Damage Cases 61

Chapter 8. CONCLUSIONS AND RECOMMENDATIONS 63

8.1 Joint Modeling Results 63

8.2 Finite Element Model Updating Using Antiresonance Results 63

8.3 Damage Detection Results 64

8.4 Conclusions and Recommendations 66

Appendix A. FLEXIBLE TRUSS EXPERIMENT MEMBER PROPERTIES 68

A.1 Element Matrices 68

A.2 Material Properties 70

A.3 Geometric Properties 70

A.3.1 Longerons 70

A.3.2 Regular and Top Battens 71

A.3.3 Mid Battens 71

A.3.4 Diagonals 71

A.3.5 50% Damaged Diagonal 72

Bibliography 73

Vita 77

List of Figures

Page

Figure 1. Baseline Model FRFs Before Updating [37] 14

Figure 2. Baseline FRFs After Updating [37] 15

Figure 3. Stiff Model FRFs Before Updating [37] 16

Figure 4. Stiff Model FRFs After Updating [37] 17

Figure 5. Diagram of Experiment Setup [37] 31

Figure 6. Top View of FTE 31

Figure 7. Vertical Plate Joint [37] 31

Figure 8. Mid-plate Joint [37] 31

Figure 9. Shaker, Accelerometers, and Top-plate Joint [37] 32

Figure 10. 12 DOF Beam Element [37] 36

Figure 11. Non-linear Stress Stiffening in Beams 37

Figure 12. Vertical Plate Joint FE Mesh 39

Figure 13. Regular Batten Joint FE Mesh 39

Figure 14. Mid-plate Joint FE Mesh 39

Figure 15. Top-plate Joint FE Mesh 39

Figure 16. Joint Model FRFs Before Updating 41

Figure 17. Mode Shape Comparison Between Stiff and Joint Models 43

Figure 18. FE Update Method Flowchart 45

Figure 19. Identified Antiresonant Frequencies Used in Updating 49

Figure 20. Non-Antiresonant Updated Joint Model FRFs 54

Figure 21. Antiresonant Updated Joint Model FRFs 55

Figure 22. Member 17 Damaged FRFs 58

List of Tables

Page

Table 1. Damage Detection Using Pattern Classifier Error Rate [37] 13

Table 2. Initial Joint Parameters 40

Table 3. Identified Natural Frequencies 47

Table 4. Estimated Standard Deviations of the Update Parameters 51

Table 5. Final Parameter Values from Antiresonant Update 52

Table 6. Final Update Parameter Values from Non-Antiresonant Update 52

Table 7. Cost Function Values Before and After Updating 53

Table 8. Damage Detection Accuracy Rates (32 Damage Cases) 60

Table 9. Damage Detection Accuracy Rates (113 Damage Cases) 61

Table 10. Damage Detection Accuracy Breakdown 61

Table 11. Damage Detection Accuracy Rates (32 Damage Cases) 65

Table 12. Damage Detection Accuracy Rates (113 Damage Cases) 65

Table 13. Damage Detection Accuracy Breakdown 65

Table 14. Aluminum Properties [37] 70

Table 15. Lexan Properties [37] 70

List of Symbols

Math Symbols

Symbol	Definition
$[]$	Matrix
$\{\}$	Vector
$()$	Indicates order of operations or *function of*
$\dot{\{\}}$	One derivative with respect to time
$\ddot{\{\}}$	Two derivatives with respect to time
$[]_{pq}$	The matrix has its pth row and q^{th} column deleted
$()_{pq}$	The pq^{th} element

English Symbols

Symbol	Definition (units)
$[C]$	Global damping matrix
d_L	Longeron rigid link dimension (in)
d_M	Lumped mass rigid link dimension (in)
d_B	Batten rigid link dimension (in)
d_K	Stiffness rigid link dimension (in) - connects diagonal to master node
d_{RB}	Regular batten rigid link dimension (in)
d_{MP}	Mid-plate rigid link dimension (in)
d_{TP}	Top-plate rigid link dimension (in)
$\{d\}$	Displacement vector
E_L	Longeron elastic modulus ($\mathrm{lb}_f/\mathrm{in}^2$)
$\{f\}$	Force input vector (lb_f)
h_{pq}	Displacement response at sensor DOF p due to actuator DOF q

$[H]$	Frequency response function (FRF) matrix
$[H]_{pq}$	The element corresponding to the pth row and q^{th} column of $[H]$
I	Second moment of area (in^4)
I_{batt}	Batten second moment of area (in^4)
$[I]$	Identity matrix
J	Scalar penalty or cost function
$[k]$	Element stiffness matrix (lb$_f$/in)
$[k_\sigma]$	Corrective element stiffness matrix for stress-stiffening (lb$_f$/in)
$[K]$	Global stiffness matrix (lb$_f$/in)
L	Length (in)
$[m]$	Element mass matrix (lb$_m$)
$[M]$	Global mass matrix (lb$_m$)
p	Sensor DOF
$\{p\}$	Modal force input vector (lb$_f$)
q	Actuator DOF
$\{q\}$	Modal displacement vector
$s = j\omega$	Laplace variable
$[S]$	Sensitivity matrix
u, v, w	Translational DOF for beam element
$[W_{\varepsilon\varepsilon}]$	Weighting matrix on measurements
$[W_{\theta\theta}]$	Weighting matrix on parameters
$x33$	The x direction DOF at node 33 in the FE model (actuator DOF)
$y36$	The y direction DOF at node 36 in the FE model (actuator DOF)

Greek Symbols

Symbol	Definition (units)
$\{\varepsilon\}$	Error vector in model update 1st order Taylor series approximation
$\{\delta z\}$	Vector of differences between experimental and modeled measurements
$\{\delta\theta\}$	Vector of parameter changes from previous iteration
$\delta\theta_j$	Perturbation in j^{th} update parameter
$\{\theta\}_0$	Vector of initial parameter values
θ_j	j^{th} update parameter
$\{\phi\}$	Eigenvector or mode shape
$\{\phi_j\}_p$	the pth element of the jth mode shape vector
$\{\eta\}$	Left eigenvector
ρ	Mass density (lb_m/in^3)
ω	Frequency (rad/sec)
ω^a	Antiresonant frequency (rad/sec)
ω_n	Natural frequency (rad/sec)
ω_n^a	Antiresonant natural frequency (rad/sec)
ζ	Modal damping factor
$[2\zeta\omega_n]$	Diagonal matrix of $2\zeta_j\omega_{n_j}$'s
λ	Eigenvalue (rad^2/sec^2)
λ^a	Antiresonant eigenvalue (rad^2/sec^2)
γ, θ, ξ	Rotational DOF for beam element (rad)

Subscripts and Superscripts

Symbol	Definition
a	Superscript on antiresonance data
b	Subscript on antiresonant eigendata
e	Subscript on experimental data
i	Subscript on eigendata
j	Subscript on update parameters
m	Subscript on modeled data
pq	Subscript meaning the pq^{th} element of a matrix

List of Abbreviations

Abbreviation	Definition
AFIT	Air Force Institute of Technology
APE	Assigned Partial Eigenstructure
ASTROS-ID	Automated Structural Optimization Software
DDE	Dynamic Data Exchange
DOF	Degrees of Freedom
EMAC	Extended Modal Amplitude Coherence
FE	Finite Element
FEM	Finite Element Method
FRF	Frequency Response Function
FTE	Flexible Truss Experiment
MAC	Modal Assurance Criterion
MATLAB^{TM}	Matrix Laboratory
MIMO	Multi-Input Multi-Output
MISO	Multi-Input Single-Output
SA 390^{TM}	Scientific Atlanta Dynamic Signal Analyzer Model 390
SDT	Structural Dynamics Toolbox^{TM}
SISO	Single-Input Single-Output

AFIT/GAE/ENY/00M-08

Abstract

The applications of antiresonant frequencies to finite element (FE) model updating are few and usually limited to numerical examples. This work uses antiresonant frequencies in the model updating of an experimental structure and analyzes the physical correctness of the updated model by using it to detect damage.

Antiresonant frequencies were used in the FE model updating of a six-meter aluminum truss. The model used rigid links to model welded and bolted joints. Rigid link dimensions were used as parameters in an iterative update based on eigenvalue and antiresonance sensitivities. The first update used 11 natural frequencies and 21 antiresonant frequencies from seven experimental frequency response functions (FRFs). The second update used only 11 natural frequencies. The antiresonant updated model produced a 46% better correlation to experimental FRFs than the non-antiresonant updated joint model.

The antiresonant updated model was used to predict FRFs for the FTE in 112 damaged configurations. Pattern classification and curve-fit algorithms for damage detection were tested. The curve-fit method correctly identified damage 92.6% of the time compared to 76.1% for the pattern classifier. The high quality of the model was attributed to the use of rigid links that were updated using antiresonant frequencies.

FINITE ELEMENT MODEL UPDATING USING ANTIRESONANT FREQUENCIES

Chapter 1 - Introduction

This chapter introduces finite element model updating and discusses some of the difficulties associated with current methods. The potential benefits of using antiresonant frequencies in model updating are also discussed. The objective of this research and an overview of the following chapters are given.

1.1 Finite Element Model Updating

The finite element method (FEM) has become the predominant method of analyzing the dynamics of modern structures. This method allows a complex continuous structure to be mathematically approximated as a discrete linear system made up of a mass, stiffness, and damping matrix. The discrete system consists of an assembly of finite elements (FEs), each of which is a model of a small part of the structure with simple geometry. The accuracy of the method improves as more elements are used [6:1].

Unfortunately, modern structures typically have complex geometries which can require hundreds of thousands of degrees of freedom (DOF) to accurately model. Even relatively simple structures may have bolted or welded connections between members which can be difficult to model without resorting to a fine FE mesh. The computational burden involved in analyzing a model of such large order can be significant. Most FE models make simplifying assumptions about the geometry and connections of a structure in order to keep the order of the model computationally manageable.

Mottershead and Friswell identified three categories of errors associated with using the FEM for modeling structural dynamics: (i) *model structure errors*, which are a result of uncertainty in

the governing physical relations. For example, modeling non-linear behavior with the linear FEM theory will produce this error; (ii) *model parameter errors* - which are a result of inappropriate boundary conditions or material property assumptions; (iii) *model order errors* - which are a result of not using a fine enough FE mesh [23:347].

For the dynamics of a FE model to correlate closely with those of an experimental structure, improvements must usually be made to reduce the errors associated with the FEM. *Model updating* has become the accepted name for using measured structural vibration data to correct the errors in FE models [25:1]. Model updating works by modifying the mass, stiffness, and damping parameters of the FE model until an improved agreement between model data and experimental data is achieved. Certainly there are system identification techniques which can produce a mathematical model which will reproduce the measured data exactly. These models are called *representational* models [9:99] and are inadequate for predicting the behavior of the system under different loadings, boundary conditions, or configurations. Therefore, the goal of FE model updating is to achieve an improved match between model and experimental data by making physically meaningful changes to model parameters which correct inaccurate modeling assumptions. Theoretically, an updated FE model can be used to model other loadings, boundary conditions, or configurations (such as damaged configurations) without any additional experimental testing [23:351]. Such models can be used to predict operational displacements and stresses due to simulated loads.

There are many different methods of finite element model updating. This thesis focuses on model update methods that are *parametric*, *modal*, *iterative*, and *sensitivity-based*. The word "parametric" describes the type of update parameters used. Parametric update methods change physical parameters (such as material properties or physical dimensions) from the FE model to improve the agreement between model and experimental data. The word "modal" describes the type of experimental data that is used to update the model. Modal methods attempt to optimize the

correlation between modeled modal data and experimental modal data (such as natural frequencies, modal damping factors, or mode shapes). The word "iterative" describes the process of model updating. Iterative methods iteratively change the update parameters to converge on a final set that optimizes correlation between modeled and experimental data. Finally, the word "sensitivity-based" describes the method used to determine the changes that are made to the update parameters during each iterative loop. In this case, modal sensitivities are used to determine changes in the update parameters. Sensitivities are defined as the ratio of the change in a measurement parameter to a small perturbation in a model update parameter. For example, the ratio of a change in the mode 1 natural frequency to the change in the Young's Modulus of the longeron material is a sensitivity.

The process of a parametric, modal, iterative, sensitivity-based update method begins with the formulation of an initial FE model using initial values for the update parameters. The modeled modal data and modal sensitivities are found using the FE model with the current update parameter values. The difference between the modeled and experimental modal data is then calculated. The model update method uses the sensitivities to determine a step in the update parameters that will reduce the difference between modeled and experimental data. The FE model is reformed using the new values of the update parameters, and the process repeats until some convergence criteria is met.

1.2 Problems with Modal Updating Methods

After compiling a comprehensive literature survey and authoring a textbook on FEM updating, Friswell and Mottershead concluded that the current state of the art in FE model updating involves using natural frequencies and possibly mode shape sensitivities to update the model [9:282]. Although modal methods seem to be the most powerful updating approach, there are three major difficulties associated with including mode shapes in the method. (i) Measured mode shapes are usually accurate to within 10% at best [9:162]. (ii) Measured mode shapes must either be expanded to the number of DOF in the FE model (using the not-yet-updated FE model)

or the FE model must be reduced to the number of measured DOF. The two approaches increase error in the mode shape data and the FE model respectively. (iii) The calculation of mode shape sensitivities is difficult (compared to natural frequency sensitivities) and must be accomplished every iteration [23:358].

Clearly, mode shapes increase error and add complexity to modal update methods. Mode shapes are often used despite these problems because the update process cannot afford a reduction in the quantity of measured data. The ability of model updating to converge on unique parameters is largely dependent on the amount of measured data available [9:201].

1.3 Antiresonance

Antiresonant frequencies are defined as the frequencies at which the magnitude of the frequency response at a measured DOF goes to zero [28:395]. In 1992 Lallement and Cogan [19] introduced the concept of using antiresonant frequencies to update FE models. The motivation for using antiresonant frequencies in updating is that they are easily and accurately measured like natural frequencies. Furthermore, unlike natural frequencies, numerous antiresonant frequencies can be measured, since every different frequency response function (FRF) between an actuator and a sensor contains another set of antiresonant frequencies. Lallement and Cogan referred to this increased amount of data as an "enlargement of the knowledge space" [19]. In 1998, Mottershead [26] showed that antiresonance sensitivities can be expressed as a linear combination of eigenvalue and mode shape sensitivities. Antiresonance sensitivities are defined as the ratio of the change in the square of an antiresonant frequency due to a small perturbation in a model update parameter. Mottershead also numerically demonstrated that the dominant contributors to the antiresonance sensitivities are the sensitivities of the nearest eigenvalues and corresponding mode shapes. Therefore, Mottershead concluded that antiresonant frequencies can be a preferred alternative to mode shape data.

1.4 Thesis Objective

Having introduced FE model updating, the problems encountered with using measured mode shapes, and the benefits of using antiresonant frequencies, the objective of this thesis can be given. The goal of this research was to extend a current iterative modal updating method to use antiresonant frequencies as a replacement for mode shape data. This objective was broken into five phases: literature review, experimental data collection, FE modeling, FE model updating, and damage detection.

FE model updating using antiresonant frequencies was applied to the modeling of the Air Force Institute of Technology (AFIT) six-meter flexible truss experiment (FTE). The updated FE model was compared to modal updated and FRF updated FE models of the same structure. Finally, the validity of the model and the updating method was evaluated by using the updated model to detect damaged members in the FTE. The ability to correctly model damaged states of the structure (states which were not involved in the updating process) was chosen to be an indicator of the success of model updating using antiresonant frequencies.

1.5 Thesis Overview

This chapter briefly introduced and motivated FE model updating using antiresonant frequencies. Chapter 2 presents related work in FE model updating, damage detection, antiresonance, previous research on the FTE, and joint modeling. Chapter 3 presents the mathematical theory for antiresonance and model updating. Chapter 4 contains a description of the FTE, the experimental setup, and the data collection methods used. Chapter 5 details the development of the FE model and the initial correlation between model and experimental data. Chapter 6 gives the results of model updating and compares the updated model to previously updated models of the FTE. Chapter 7 applies the updated model to the problem of damage detection and compares the results to previous damage detection results. Chapter 8 presents the conclusions and recommendations from this research.

Chapter 2 - Background

This chapter contains a literature review on subjects related to this thesis. The topics of model updating, damage detection, antiresonance, previous research on the FTE, and joint modeling are covered. Lastly, these areas are summarized and the contributions of this research are stated.

2.1 Finite Element Model Updating

Mottershead and Friswell authored two excellent references, a literature survey [23] and a textbook [9], on the subject of model updating. In their text, Mottershead and Friswell divided model updating methods into three categories: direct modal methods, FRF methods, and iterative modal methods. The following three paragraphs contain a summary of these methods based on Mottershead and Friswell's text.

Direct modal methods have the advantage in many cases of exactly reproducing the experimental data without iteration and excessive computation. However, they often have the disadvantage of updating the mass and stiffness matrices directly so that the changes may have little physical meaning to the original FE model. Examples of direct methods are Lagrange multiplier methods, optimal orthogonalization of the modal matrix, and eigenstructure assignment. Mottershead and Friswell [9:137] provide a table comparing the various cost functions, constraints, and update equations that define the numerous direct modal methods.

FRF methods use the FRF data to update the FE model. These methods have the advantage of using measured data directly. The major disadvantage of FRF update methods is that damping must be included in the FE model. Typically, model updating is concerned with finding the correct mass and stiffness parameters of the model and not the correct damping parameters. In fact, damping is notoriously difficult to model accurately, and any changes to damping parameters made by updating may not be physically significant [9:281]. Moreover, although FRFs contain more data points than modal data, they do not contain significantly more information.

Iterative modal methods are popular and frequently used methods that use eigenvalue and mode shape sensitivities to minimize some cost function. Often this cost function is simply the sum of squares of the difference between experimental and modeled natural frequencies and mode shapes. Typically, the cost function is a non-linear function of the update parameters. Therefore, these methods generally use a truncated Taylor series expansion of the modal data in terms of the update parameters. Small iterative steps are taken with sensitivities recalculated at every iteration until the non-linear cost function is minimized. This method has the advantage of allowing any parameter in the FE model to be used as an update parameter since the FE model is reconstructed and an eigenanalysis accomplished at every iteration. Obviously, this method can become computationally burdensome for large FE models. However, the eigendata sensitivities generally converge the update parameters within a reasonable number of iterations.

An iterative modal method, called the penalty method, was chosen for this research for two reasons. First, the penalty method could easily be extended to include antiresonant frequencies in updating. Second, it allowed the geometric dimensions of the joints to be used as update parameters.

2.2 Damage Detection

Damage detection provides an excellent indication of model quality when damaged data is not used in updating. Because damage detection was used in this thesis as a test for model quality, this literature review focuses on the reliance of damage detection methods on FE models and the errors that inaccurate FE models cause.

Damage Detection using vibration data has been a very active research topic for the last 30 years [37:1]. Doebling, *et al.* [7] has written a thorough review of current damage detection methods which shows that most methods rely heavily on some numerical model of the structure. For example, early damage detection methods directly updated the mass and stiffness matrices based on experimental data from the damaged structure. There were significant problems with that

technique, and most current methods now rely on updating parametric FE models [10:3]. Other methods rely on FE models to create a catalog of FRFs or modal data for the various damage cases. Neural networks have recently been applied to damage detection, and they also typically require FE models to produce training data for damage states [7].

Friswell and Penny [10:5] called the reliance on FE models a major problem with damage detection. Damage detection techniques have difficulty distinguishing whether discrepancies between modeled and experimental data are due to damage or due to modeling errors. Friswell and Penny identified model updating as a critical approach to reducing this problem. Both Doebling, *et al.* [7] and Friswell and Penny [10] concluded that there is a need for damage detection techniques to be tested on experimental structures rather than using numerical simulations.

2.3 Antiresonance

Antiresonance is often presented in vibrations textbooks in the design of vibration absorbers [21:131]. An example of this type of research was conducted by He and Li [14]. They were able to relocate antiresonances of a vibrating system by making local changes to the mass and stiffness of the vibrating system. They applied the theory to numerical examples, including a four DOF system and an eight DOF truss model. Mottershead [27] established the necessary and sufficient conditions to cancel a natural frequency with an antiresonance. Such a cancellation is sometimes referred to as *pole-zero cancellation*. Pole-zero cancellation removes the large amplitude resonant response normally associated with excitation near a natural frequency.

Williams and Juang [43] researched flexible space structures with collocated sensors and actuators from a control system perspective. They were able to relocate transmission zeros to produce pole-zero cancellations. They proved that the closed loop poles produced by applying pole-zero cancellation have sensitivities approaching those of the transmission zeros. Schrader and Sain [34] authored a survey on research on system zeros. Their development and discussion

of the subject focused on state space formulations and addressed topics such as the transmission zeros for multi-input multi-output (MIMO) systems.

Tohyama and Lyon [38] analyzed the zeros of transfer functions in multi-DOF vibrating systems. They analyzed the different types of zeros present in transfer functions such as conjugate zero pairs, coincident double zeros, minimum phase zeros, and non-minimum phase zeros. Numerical examples were presented using the transfer function of a rectangular room. Methods of identifying the different types of zeros from frequency response plots were also included.

Wahl, *et. al.* [40], addressed the physical significance of resonance-antiresonance behavior in lightly damped structures. They stated that the antiresonant frequencies of the driving point FRF (an FRF between a collocated actuator and sensor) are identical to the resonance frequencies of the structure that is fixed at the driving point DOF. Therefore, with one test it is possible to gain information about the structure under two sets of boundary conditions. Analogous statements about multi-input systems were developed. The effect of local structural mass and stiffness changes on antiresonant frequencies was also discussed. Experimental investigations were conducted on a steel plate. They concluded that antiresonance behavior has important applications to FE model updating.

La Civita and Sestieri [18] investigated the physical interpretation of antiresonance in continuous one-dimensional systems. Antiresonant frequencies were found to correspond to resonances frequencies of particular substructures. These substructures and their boundary conditions were defined. The correspondence was exact for multi-DOF one-dimensional systems and longitudinal rods and approximate for beams.

Feng-Quan, *et. al.* [8] compared the analytical development of the transfer function of an undamped cantilever steel beam to experimental data. They analyzed the antiresonance characteristics of the beam as well as defined pseudo-resonance as the appearance of an extreme value (which is not a resonance) between two antiresonant frequencies.

Rogers [33] first derived the general eigenvalue and eigenvector derivatives of non-symmetric matrices, which can be applied to the calculation of antiresonance sensitivities. Wang [41] developed a thorough theory of antiresonance and antiresonance sensitivity analysis. Antiresonant frequencies for any responses that are a linear combination of displacement responses at different DOF were found for arbitrary forcing functions. Formulas for antiresonant response modes (which are analogous to mode shapes) and their sensitivities were also presented. Wang applied his theory to the numerical example of a beam, a plate, and a 10 DOF spring-mass system.

Lallement and Cogan [19] applied antiresonant frequencies to FE model updating. They developed an iterative parametric update technique which combined eigenvalue sensitivities, antiresonance sensitivities, orthogonality relations, and dynamic flexibility relations into one non-homogeneous linear system of the form $[A]\{x\} = \{b\}$, where $\{x\}$ is a vector of update parameters and $\{b\}$ is a vector of discrepancies between model and measured data. Rade, *et. al.* [30] built on this concept by considering the *generalized grounding of DOF*. The generalized grounding of DOF was defined as the elimination of dynamic response at one or several DOF for a convenient system of control forces. The eigendata for a structure with zero dynamic response at several DOF's was obtained from an eigensolution of submatrices of the dynamic flexibility matrix. This method allowed the system to be considered under several different boundary conditions using data from only one test configuration. Rade, *et. al.* incorporated the increased set of data into a linear system in the form $[A]\{x\} = \{b\}$ as Lallement and Cogan [19] had done. The technique was applied to a real structure as well as simulated numerical examples of a free-free beam and a frame structure. The new information attained from antiresonances or new generalized boundary conditions dramatically improved the ability of model updating to converge on the correct parameter values. Also, it was demonstrated that, in some cases, antiresonances are much more sensitive to parameter changes than natural frequencies.

Mottershead [26] analyzed the sensitivities of antiresonances and expressed them as functions of the eigenvalues and mode shapes of a structure. He demonstrated, through a numerical example, that the dominant contributors to the antiresonance sensitivities are the sensitivities of the nearest eigenvalues and corresponding mode shapes. He concluded that antiresonances are not independent of the structural eigendata, but antiresonances may be a preferred alternative to using mode shapes because of the accuracy with which they can be measured.

2.4 Previous Research on the Flexible Truss Experiment

The FTE was originally part of the 12-Meter Truss Active Vibration Control Experiment developed for the Wright Laboratories Large Space Structures Technology Program [12]. The FTE was given to AFIT where it is currently set up as a 6-Meter truss.

Several FE models of the FTE have been created. Two FE models of the 12-meter version were created for the 12-Meter Truss Active Control Experiment [12] to predict its open-loop response. The first model represented the truss as a frame structure with 192 beam elements and 384 active DOF. Each truss member was modeled as a two-noded beam element with 6 DOF per node. The four nodes at the base were fixed to simulate the cantilever boundary condition. The actuators were modeled as single DOF spring mass damper systems with 1.0 Hz natural frequencies and 10% modal viscous damping. This model did not predict the natural frequencies of the truss well. The predicted bending mode frequencies of the model were too high by 10% and the torsional mode frequencies were too low by 10%. The truss was also tested and modeled in a free-free configuration (supported by soft springs) with similar discrepancies reported. Attempts to find a physically meaningful combination of parameters that would soften the bending modes but stiffen the torsion modes were unsuccessful.

An equivalent continuous beam FE model was developed as part of the same experiment. Each of the 16 bays were modeled as a single beam element resulting in a 16 element, 33 node, and 136 DOF model. Element properties were found by applying axial, bending, torsion, and

shear loads to a detailed model of a single truss bay. The initial beam model agreed well with measured data through the third bending modes.

Captain Richard Cobb studied damage detection on the 6-meter FTE. Cobb modeled the FTE as a frame structure with joints modeled by a single node. Cobb's model, called the *baseline model*, had 36 nodes and 192 DOF. Cobb used the first eight natural frequencies and mode shapes to update 23 parameters using a software package called Automated Structural Optimization Software (ASTROS-ID). Cobb had trouble extracting measured mode shapes for model updating and damage detection due to closely spaced fourth and fifth modes (first breathing and second bending modes). He was forced to use his FE model to uncouple the mode shapes. This illustrated the type of problems encountered when using mode shapes in model updating and damage detection. The update process converged in six iterations and 18 minutes on a SPARC 10 workstation. Figure 1 and Figure 2 contain FRFs from the baseline before and after tuning.

Cobb developed a new assigned partial eigenstructure (APE) method to detect damage on the FTE. Cobb tested 2 simulated damage cases, one diagonal fully removed, and one diagonal replaced with a diagonal of 50% of normal cross sectional area. In both cases, the method was able to correctly identify the small area of the truss where the damaged member was and approximate the percentage of damage. The damage detection calculations took approximately 9 minutes on a SPARC 20 workstation.

Captain Eric Swenson used pattern classifiers to detect damage on the FTE. He created a new finite element model, called the *stiff model*, which used short stiff beam elements to model the joints of the FTE. This increased the size of the model to 996 DOF. Swenson found that the position of the diagonal endpoint nodes was critical to accurately model the torsional modes of the FTE. This was because the diagonals are capped with solid aluminum ends, which are relatively heavy. These heavy ends were modeled as lumped masses, which, if placed at corner joint nodes, produced torsional modes that were too low in frequency. Swenson was able to lump these masses

in their realistic locations, reducing the torsional inertia of the structure, and raising the torsional natural frequency to match experimental data. However, this required relatively long stiff elements which overstiffened the joints. Swenson compensated by reducing the stiffness of his stiff elements to give a good initial fit between the modeled and experimental FRFs. Swenson used the FRF based model updating routine from the MATLAB^{TM} Structural Dynamics Toolbox^{TM} (SDT) to update 9 parameters. The update took approximately 15 hours to converge to a solution on a SPARC 20 workstation. Figure 3 and Figure 4 show the stiff model before and after updating.

The updated stiff model showed a considerably better fit than the updated baseline model. However, the antiresonances of the updated models did not match the experimental antiresonances well. The modal updated baseline model produced better damage detection results than the FRF updated stiff model. Damage detection results are included in Table 1. Swenson concluded that the low damage detection accuracy rates were due to FE model errors, since the pattern classifier was able to correctly identify damage 100% of the time when using the experimental data for the 32 damage cases. Swenson concluded that the FTE joints were the source of most of the model errors.

Table 1. Damage Detection Using Pattern Classifier Error Rate [37]

	Modal-Updated Baseline Model	FRF-Updated Stiff Model
Initial error rate	18%	23%
Related member errors	15%	9%
Unbroken errors	2%	10%
Unrelated errors	1%	4%

2.5 Joint Modeling

The joints are typically the most difficult part of a truss to model [17]. In addition to the complex geometry, joints exhibit non-linear behavior such as the microscopic slip in bolted connections [29]. Suarez and Matheu [36] have shown that joint flexibility can have a significant effect on a structure's dynamics.

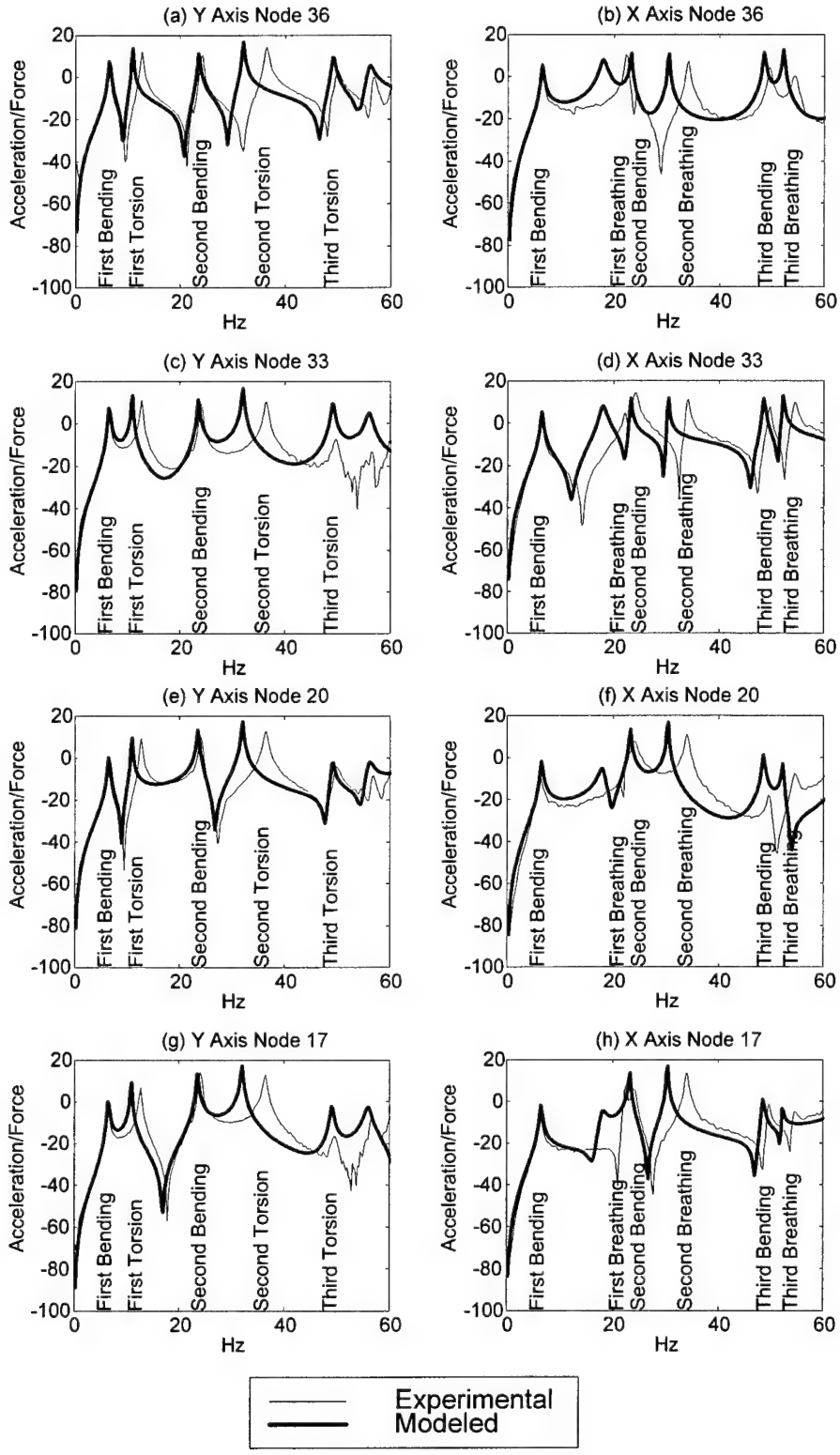

Figure 1. Baseline Model FRFs Before Updating [37]

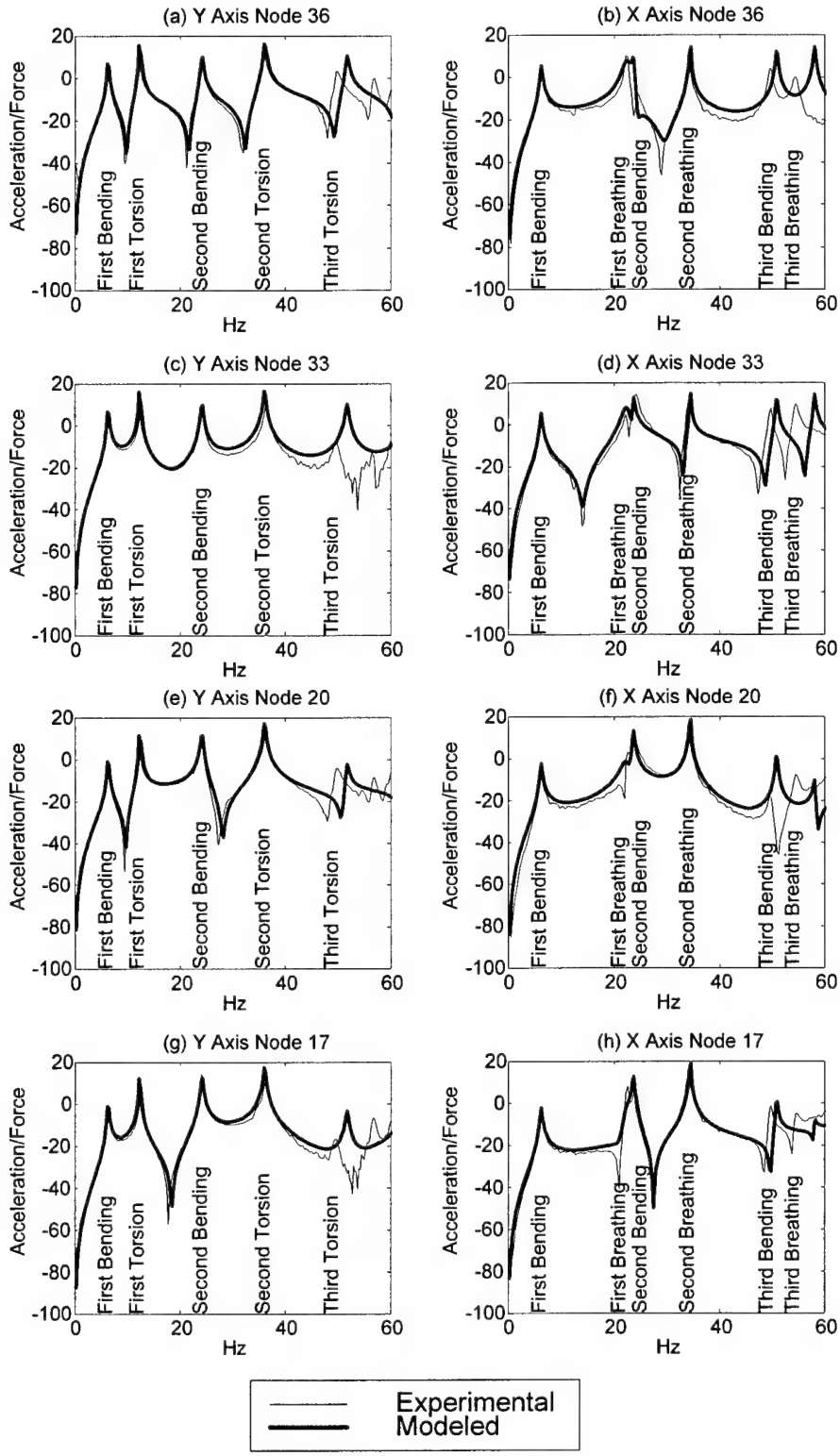

Figure 2. Baseline FRFs After Updating [37]

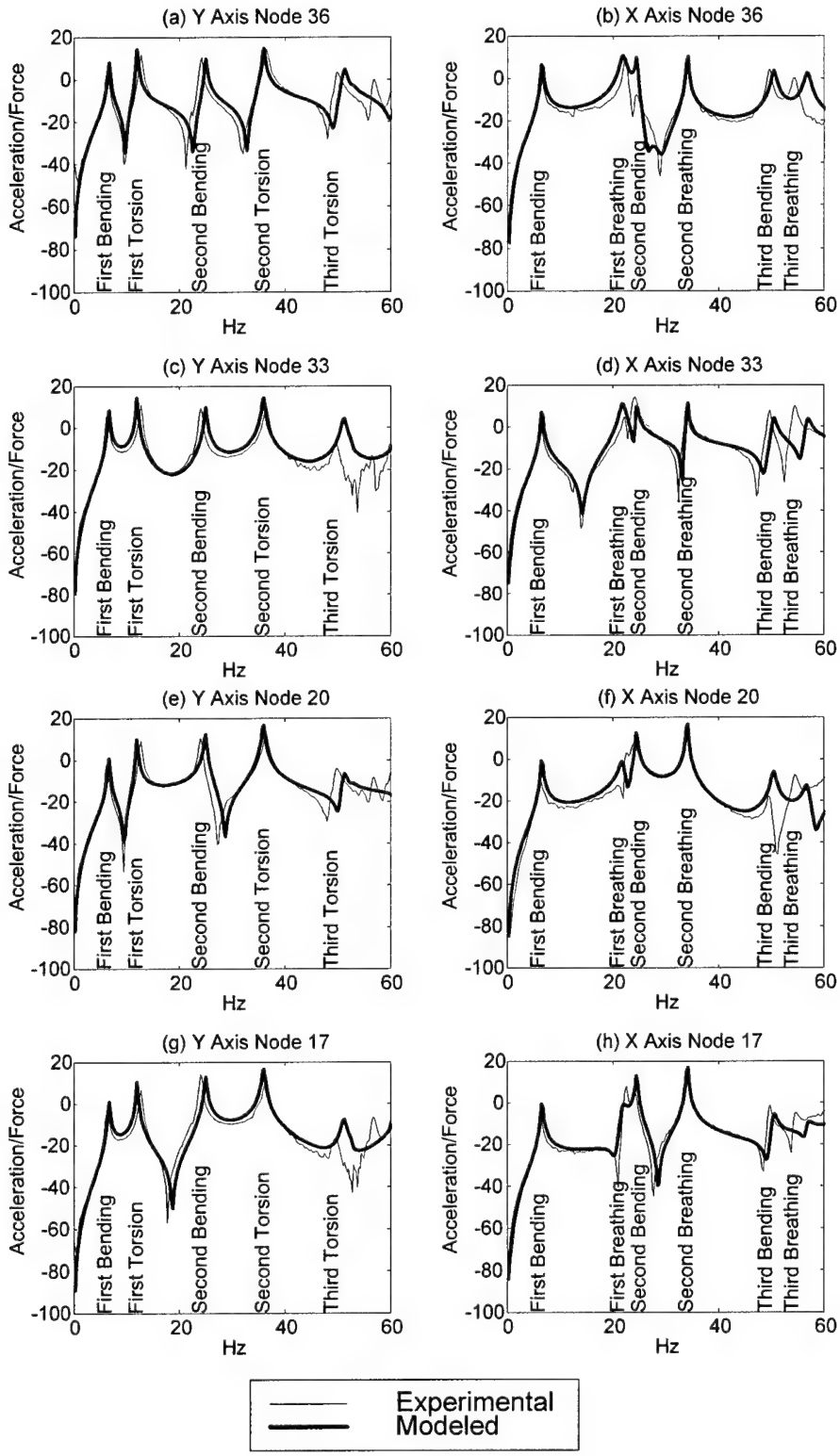

Figure 3. Stiff Model FRFs Before Updating [37]

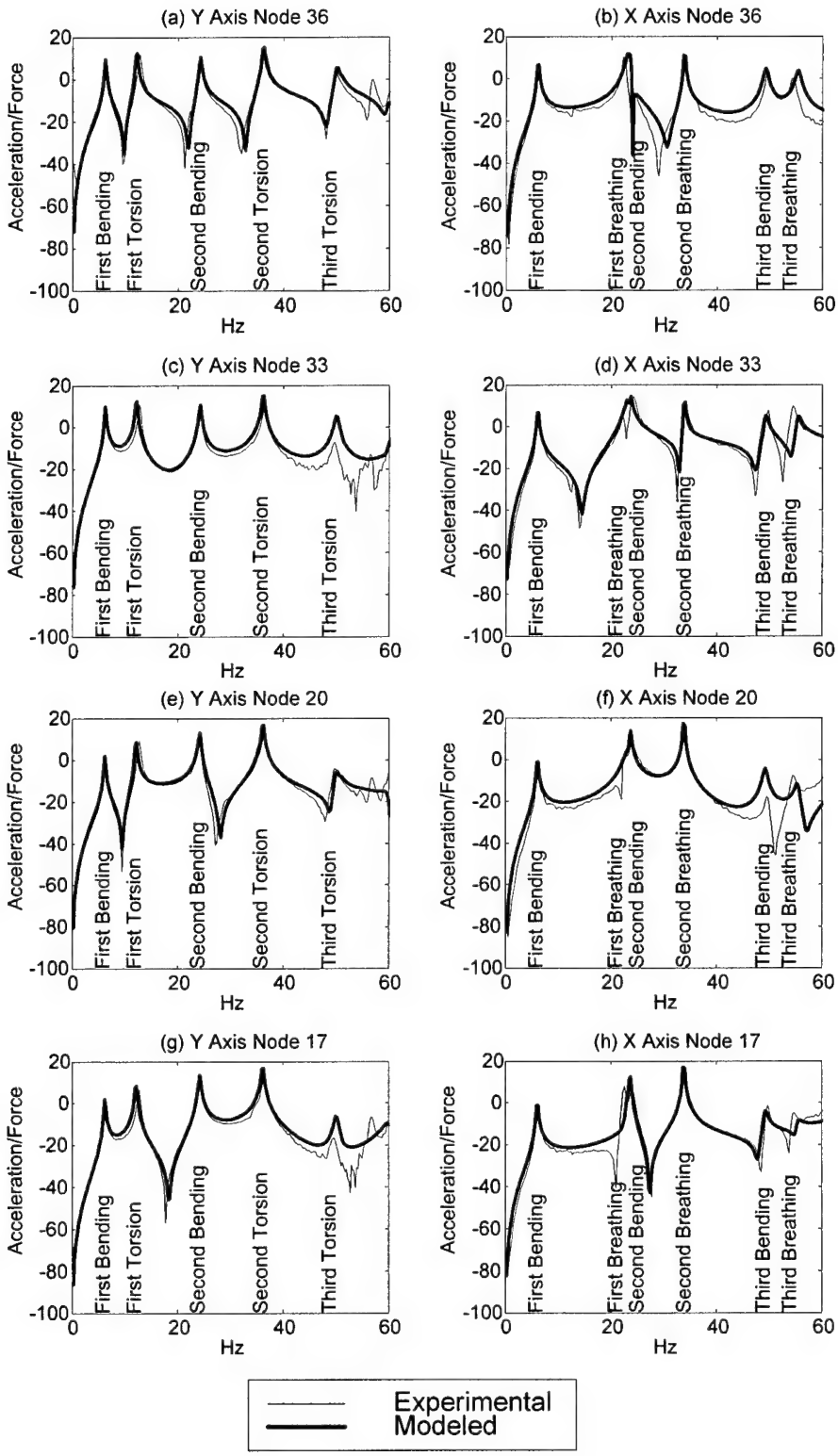

Figure 4. Stiff Model FRFs After Updating [37]

Research has been conducted into how to model structural joints accurately without resorting to detailed FE meshes. One approach taken by Kienholtz [17] was to build physical scale models of structural joints. Belvin [4] used linear springs and dashpots, and non-linear creep and friction elements, in order to create linear and non-linear analytical models of joints. The properties of the analytical joint models were determined using experimental data from load-deflection testing. This method has the disadvantages of requiring experimental data on the joint, introducing damping into the FE analysis, and possibly requiring a non-linear FE analysis.

When the joints cannot be separated from the structure for testing, other methods are required. Wang and Sas [42] developed a method which uses an approximate eigenvector of the structure to iteratively converge on a single joint's parameter values. This method assumed all the physical parameters of the system were known except for those associated with the joint. Tsai and Chou [39] developed a method to identify the dynamic characteristics of a single bolted joint from the measured FRFs of substructures and the assembled structure. This method required the isolation of substructures from the rest of the system, but had the advantage of not requiring sensors to be near the joint.

Mottershead, *et. al.* [24] developed an approach to joint modeling which used geometric offsets to parameterize multiple joints in a structure. Rigid elements were used to connect nodes displaced by a geometric offset. Two FE models of a beam with welded flanges, one with rigid links connecting offset nodes and another with translational and rotational springs connecting offset nodes, were compared. The eigenvalues of the modeled beam were shown to be more sensitive to geometric offset parameters than to spring constant or beam thickness parameters. Ahmadian, *et. al.* [2] reformulated the concept of geometric offsets into a partly rigid beam element for FE models. Horton, *et. al.* [15] compared model updating of the welded joints in a tubular H frame with joints parameterized with either springs or geometric offsets. Better update results were achieved using geometric offsets.

Geometric offsets were chosen to model and update the FTE joints in this thesis. This method was chosen based on the successful use of geometric offsets to model joints by Mottershead, *et. al.* [24], Ahmadian, *et. al.* [2], and Horton, *et. al.* [15]. Geometric offsets were particularly attractive, because they do not add DOF to the FE model. Furthermore, geometric offsets have the physical meaning of expanding and contracting the rigid area of the joint as the offset parameters change during updating.

2.6 Summary

Model updating and damage detection are two rapidly progressing areas of research. Lament and Cogan [19] and Rade, *et. al.* [30] have applied antiresonance to model updating and shown its potential benefits. However, the applications of antiresonance to model updating are few and usually limited to numerical examples. This thesis applies model updating using antiresonance to an experimental structure, compares the method to model updating using only natural frequencies, and analyzes the physical correctness of the updated model by using it to detect damage. Also, both Doebling *et. al.* [7] and Friswell and Penny [10] have cited the need for studies that test damage detection methods on experimental rather than simulated structures, and for studies that directly compare damage detection methods. This thesis tests two FRF based damage detection methods, a pattern classifier method and a curve-fit method, on an experimental structure and compares results.

Chapter 3 - Theory

This chapter contains the mathematical theory behind model updating and antiresonance. First, the relationship between antiresonant frequencies and mode shapes is explained to provide the motivation for using antiresonant frequencies in model updating. The equations used in model updating, including those for the calculation of antiresonant frequencies, eigenvalue and antiresonant eigenvalue sensitivities, and the tracking of modes, are presented.

3.1 Antiresonance / Mode Shape Relationship

The displacement response at DOF p due to a unit harmonic force input at DOF q for a FE model with no repeated eigenvalues can be written as [9:23]:

$$H_{pq}(\omega) = \sum_{j=1}^{r} \frac{\{\phi_j\}_p \{\phi_j\}_q}{\omega_{n_j}^2 - \omega^2 + 2i\zeta_j\omega_{n_j}\omega} \tag{1}$$

where

p = measured DOF

q = input force DOF

r = number of modes

$\{\phi_j\}_p$ = the pth element of the jth mode shape vector

ω_{n_j} = the jth natural frequency

ω = input forcing frequency

ζ_j = the jth modal damping factor

$i = \sqrt{-1}$

A close inspection of (1) shows that the magnitude of the FRF will become very large as ω approaches ω_{n_j} (assuming ζ_j's are very small for structures). This phenomena is called *resonance*. Antiresonance is defined as the frequency at which the FRF goes to zero [28:395].

For a frequency ω between two natural frequencies, ω_{n_j} and $\omega_{n_{j+1}}$, the magnitude of the FRF will typically be dominated by the contributions from modes j and $j+1$. Considering only these

two dominant terms in an undamped system, equation (1) can be written as:

$$H_{pq}(\omega) = \frac{\{\phi_j\}_p \{\phi_j\}_q}{\omega_{n_j}^2 - \omega^2} + \frac{\{\phi_{j+1}\}_p \{\phi_{j+1}\}_q}{\omega_{n_{j+1}}^2 - \omega^2} \tag{2}$$

From (2) it is easy to see that if the products $\{\phi_j\}_p \{\phi_j\}_q$ and $\{\phi_{j+1}\}_p \{\phi_{j+1}\}_q$ are the same sign, there exists an antiresonant frequency ω^a between ω_{n_j} and $\omega_{n_{j+1}}$, where $h_{pq}(\omega^a) = 0$. Furthermore, consider the case of a collocated actuator and sensor $p = q$. Then $\{\phi_j\}_p \{\phi_j\}_q = \{\phi_j\}_p^2$, which is positive for all j. Therefore, the collocated case produces an antiresonance between every two resonant peaks and the resonances and antiresonances will interlace. For non-collocated actuators and sensors $p \neq q$, no such interlacing property generally exists.

For an undamped structure, the FRF can be formulated as the following transfer function between a sensor p and an actuator q [1]:

$$H_{pq}(s) = \frac{k \prod_{i=1}^{m} \left(s^2 + (\omega_i^a)^2\right)}{\prod_{j=1}^{n} \left(s^2 + (\omega_{n_j})^2\right)} \tag{3}$$

where

k = a constant coefficient

m = the number of second order zeros

n = the number of second order poles

$s = jw$ the Laplace variable

Equation (1) shows that the FRF is completely defined by the natural frequencies and mode shapes of the system (ignoring damping). Equation (3) shows that the FRF is completely defined by the natural frequencies and antiresonant frequencies of the system. Therefore, the antiresonances must contain information about the mode shapes of a system. This demonstrates that antiresonance can be used as an indirect (but perhaps more accurate) way to update FE model mode shapes to match experimental mode shapes. Mottershead confirmed this fact by formulating the antiresonance sensitivities as a function of the eigenvalues and mode shape sensitivities of a structure [26].

3.2 Calculating Antiresonant Frequencies

Antiresonant frequencies could be solved from either (1) or (3) by setting $h_{pq} = 0$. However, this method would require knowledge of the modal damping factors and truncation to keep the problem computationally manageable. To develop a more accurate and efficient method of calculating the antiresonances, consider the following development taken from He and Li [14]. Start with the undamped FE equation of motion in the time domain:

$$[M]\{\ddot{d}\} + [K]\{d\} = \{f\} \tag{4}$$

For a force vector $\{f\} = \{F\}\sin\omega t$ resulting in harmonic response $\{d\} = \{D\}\sin\omega t$, (4) becomes:

$$([K] - \omega^2[M])\{D\} = \{F\} \tag{5}$$

Therefore the response $\{D\}$ of the system is:

$$\{D\} = ([K] - \omega^2[M])^{-1}\{F\} \tag{6}$$

The FRF matrix $[H(\omega)]$ is typically defined as:

$$[H(\omega)] = ([K] - \omega^2[M])^{-1} \tag{7}$$

The FRF for a sensor at DOF p and an actuator at DOF q will be the pq^{th} element of $[H]$:

$$H_{pq}(\omega) = ([K] - \omega^2[M])^{-1}_{pq} = \frac{adj([K] - \omega^2[M])_{pq}}{\det([K] - \omega^2[M])} \tag{8}$$

The adjoint is defined as the transpose of the cofactor of a matrix. The cofactor of a matrix $[A]$ is:

$$C_{pq} = (-1)^{p+q}\det([A]_{pq}) \tag{9}$$

where $[A]_{pq}$ denotes that row p and column q have been deleted from the matrix. Therefore, (8) can be written as:

$$H_{pq}(\omega) = (-1)^{p+q}\frac{\det([K]_{pq} - \omega^2[M]_{pq})}{\det([K] - \omega^2[M])} \tag{10}$$

where $[K]_{pq}$ and $[M]_{pq}$ denote that row p and column q have been deleted from the matrices. The antiresonances are the positive roots of the numerator of (10). Therefore the antiresonant frequencies ω^a for the FRF between p and q are the positive roots of the following equation:

$$\det([K]_{pq} - (\omega^a)^2[M]_{pq}) = 0 \tag{11}$$

We define the *antiresonant eigenvalues* as the squares of these roots ($\lambda^a = (\omega^a)^2$). If damping were included in this development, the roots of equation (11) would be *antiresonant natural frequencies* ω_n^a, and the antiresonant eigenvalues would be defined as $\lambda^a = (\omega_n^a)^2$. For the undamped case, antiresonant frequencies and antiresonant natural frequencies are the same, just as resonant frequencies and natural frequencies are the same.

Equation (11) has the interesting interpretation that the antiresonant frequencies for an FRF between p and q are the natural frequencies of the system with row p and column q removed from the mass and stiffness matrices. Notice that, for a collocated sensor and actuator FRF $p = q$, the same row and column are deleted from $[M]$ and $[K]$, and the matrices remain symmetric. Therefore, the antiresonant eigenvalues of collocated FRFs are always real numbers. In the case of non-collocated sensors and actuators $p \neq q$, $[M]$ and $[K]$ are, in general, not symmetric, and the antiresonant eigenvalues can be real or complex conjugates [44:435-438].

For this thesis, an eigenanalysis of $[M]_{pq}$ and $[K]_{pq}$ was used to calculate antiresonant frequencies during model updating. The MATLAB^{TM} function *eigs* was used to extract the low frequency antiresonant eigenvalues from the unsymmetric matrices [20]. The MATLAB^{TM} SDT subspace iteration eigensolver was used to extract the low frequency eigenvalues from the symmetric $[M]$ and $[K]$ matrices [3].

3.3 Model Updating - Penalty Method

The *penalty method* is a frequently used method for updating FE models using the sensitivities of modal data. This development of the penalty method was taken from Friswell and Mottershead's text on FE model updating [9].

The first step in FE updating is to decide upon which data to compare in updateing the model. The penalty method can use eigenvalues, mode shapes, and modal damping factors, but for this thesis only eigenvalues are used. The error between the experimental and modeled eigenvalues is

defined as:

$$\delta z_i = \lambda_{e_i} - \lambda_{m_i} \qquad i = 1 \ldots n \tag{12}$$

where the subscript e denotes *experimental*, m denotes *modeled*, and n is the number of eigenvalues being used to update the model. Then the perturbation in the update parameters is defined as:

$$\delta\theta_j = \theta_{new_j} - \theta_{old_j} \qquad j = 1 \ldots r \tag{13}$$

where r is the number of update parameters. A 1st order Taylor series expansion is used to relate δz_i to $\delta\theta_j$:

$$\delta z_i \approx \frac{\partial \lambda_i}{\partial \theta_1}\delta\theta + \frac{\partial \lambda_i}{\partial \theta_2}\delta\theta + \cdots + \frac{\partial \lambda_i}{\partial \theta_r}\delta\theta \qquad i = 1 \ldots n \tag{14}$$

Equation (14) can be written in matrix form as:

$$\{\delta z\}_{n\text{x}1} \approx [S]_{n\text{x}r}\{\delta\theta\}_{r\text{x}1} \tag{15}$$

$$[S] = \begin{bmatrix} \frac{\partial \lambda_1}{\partial \theta_1} & \cdots & \frac{\partial \lambda_1}{\partial \theta_r} \\ \vdots & \ddots & \vdots \\ \frac{\partial \lambda_n}{\partial \theta_1} & \cdots & \frac{\partial \lambda_n}{\partial \theta_r} \end{bmatrix} \tag{16}$$

$[S]$ is called the sensitivity matrix because it contains the sensitivities of each eigenvalue to each update parameter. Subtracting $[S]\{\delta\theta\}$ from both sides gives the error $\{\varepsilon\}$ in the 1st order Taylor series approximation:

$$\{\varepsilon\} = \{\delta z\} - [S]\{\delta\theta\} \approx \{0\} \tag{17}$$

The scalar penalty function J is constructed from the weighted sum of squared errors in the predicted measurements $\{\varepsilon\}$. In order to make this set of equations well conditioned, the weighted deviation from the initial update parameters is added to the penalty function J. This reflects the desire for a solution that reproduces the experimental data by changing the update parameters as little as possible. The penalty function is:

$$J = \{\varepsilon\}^T [W_{\varepsilon\varepsilon}]\{\varepsilon\} + \{\{\theta\} - \{\theta\}_0\}^T [W_{\theta\theta}] \{\{\theta\} - \{\theta\}_0\} \tag{18}$$

where

$[W_{\varepsilon\varepsilon}]$ = weighting matrix on the measured eigenvalues

$[W_{\theta\theta}]$ = weighting matrix on the update parameters

$\{\theta\}_0$ = initial values of the update parameters

The penalty function J can be minimized with respect to the update parameters by setting the derivative of J with respect to the update parameters equal to zero and solving for $\{\delta\theta\}$. The resulting solution for the set of update parameters that minimizes the penalty function is:

$$\{\delta\theta\} = \left[[S]^T [W_{\varepsilon\varepsilon}] [S] + [W_{\theta\theta}]\right]^{-1} \left\{[S]^T [W_{\varepsilon\varepsilon}] \{\delta z\} - [W_{\theta\theta}] \{\{\theta\} - \{\theta\}_0\}\right\} \tag{19}$$

This equation is iteratively applied, recalculating $[S]$ at every iteration, until the update parameters converge.

3.4 Penalty Method Extended to Include Antiresonant Frequencies

The penalty method can easily be extended to include antiresonant frequencies in model updating. The antiresonant eigenvalues are defined as the antiresonant frequencies (measured experimentally) squared. The modeled antiresonant eigenvalues come from the eigenanalysis of (11). The penalty method including antiresonances can be written as:

$$\delta z_b^a = \lambda_{e_b}^a - \lambda_{m_b}^a \qquad b = 1 \ldots k \tag{20}$$

$$\{\delta z\}^* = \left\{ \begin{array}{c} \{\delta z\}_{n\text{x}1} \\ \{\delta z^a\}_{k\text{x}1} \end{array} \right\} \approx [S]^*_{(n+k)\text{x}r} \{\delta\theta\}_{r\text{x}1} \tag{21}$$

$$[S]^* = \begin{bmatrix} \frac{\partial\lambda_1}{\partial\theta_1} & \cdots & \frac{\partial\lambda_1}{\partial\theta_r} \\ \vdots & \ddots & \vdots \\ \frac{\partial\lambda_n}{\partial\theta_1} & \cdots & \frac{\partial\lambda_n}{\partial\theta_r} \\ \frac{\partial\lambda_1^a}{\partial\theta_1} & \cdots & \frac{\partial\lambda_1^a}{\partial\theta_r} \\ \vdots & \ddots & \vdots \\ \frac{\partial\lambda_k^a}{\partial\theta_1} & \cdots & \frac{\partial\lambda_k^a}{\partial\theta_r} \end{bmatrix} \tag{22}$$

where k is the number of antiresonant eigenvalues used to update the model. The penalty method is solved iteratively in the same way, according to (19).

3.5 Eigenvalue Sensitivities

The eigenvalue sensitivities required in equation (22) can be derived from the standard eigenproblem [22:126]:

$$([K] - \lambda_i [M]) \{\phi_i\} = 0 \tag{23}$$

Differentiation of (23) with respect to an update parameter θ_j gives:

$$([K] - \lambda_i [M]) \frac{\partial \{\phi_i\}}{\partial \theta_j} + \left(\frac{\partial [K]}{\partial \theta_j} - \lambda_i \frac{\partial [M]}{\partial \theta_j} - \frac{\partial \lambda_i}{\partial \theta_j} [M] \right) \{\phi_i\} = 0 \tag{24}$$

Pre-multiplying (24) by $\{\phi_i\}^T$ gives:

$$\{\phi_i\}^T ([K] - \lambda_i [M]) \frac{\partial \{\phi_i\}}{\partial \theta_j} + \{\phi_i\}^T \left(\frac{\partial [K]}{\partial \theta_j} - \lambda_i \frac{\partial [M]}{\partial \theta_j} - \frac{\partial \lambda_i}{\partial \theta_j} [M] \right) \{\phi_i\} = 0 \tag{25}$$

The first term in (25) is equal to zero by (23). Solving for the eigenvalue sensitivity gives:

$$\frac{\partial \lambda_i}{\partial \theta_j} = \frac{\{\phi_i\}^T \left(\frac{\partial [K]}{\partial \theta_j} - \lambda_i \frac{\partial [M]}{\partial \theta_j} \right) \{\phi_i\}}{\{\phi_i\}^T [M] \{\phi_i\}} \tag{26}$$

The mass and stiffness matrices sensitivities can be found by finite differencing [22:125]:

$$\frac{\partial [K]}{\partial \theta_j} \approx \frac{[K(\theta_{0_j} + \delta\theta_j)] - [K(\theta_{0_j})]}{\delta\theta_j} \tag{27}$$

$$\frac{\partial [M]}{\partial \theta_j} \approx \frac{[M(\theta_{0_j} + \delta\theta_j)] - [M(\theta_{0_j})]}{\delta\theta_j} \tag{28}$$

Finite differencing allows any FE parameter to be used as an update parameter without having to analytically derive the mass and stiffness sensitivities. This allows different choices in update parameters to be quickly studied. The speed of the algorithm can be improved for a particular set of update parameters by using analytical mass and stiffness sensitivities.

3.6 Antiresonance Sensitivities

Antiresonant eigenvalue sensitivities are also required in equation (22). As seen previously, antiresonant eigenvalues can be found from the eigenanalysis of $[M]$ and $[K]$ where the row corresponding to the sensor DOF p and the column corresponding to the actuator DOF q are deleted. $[M]_{pq}$ and $[K]_{pq}$ will no longer be symmetric matrices in general. Notice that $\{\phi_i\}^T ([K] - \lambda_i [M])$ in (25) is not equal to zero by (23) if $[M]_{pq}$ and $[K]_{pq}$ are not symmetric. Therefore, the antiresonant eigenvalue sensitivities require a slightly different derivation than

the eigenvalue sensitivities. Equations (23) and (24) can be rewritten for the antiresonant eigenproblem as:

$$\left([K]_{pq} - \lambda_b^a [M]_{pq}\right) \{\phi_b\} = 0 \tag{29}$$

$$\left([K]_{pq} - \lambda_b^a [M]_{pq}\right) \frac{\partial \{\phi_b\}}{\partial \theta_j} + \left(\frac{\partial [K]_{pq}}{\partial \theta_j} - \lambda_b^a \frac{\partial [M]_{pq}}{\partial \theta_j} - \frac{\partial \lambda_b^a}{\partial \theta_j} [M]_{pq}\right) \{\phi_b\} = 0 \tag{30}$$

where λ_b^a is an antiresonant eigenvalue, and the subscripts pq denote that row p and column q have been deleted from $[M]$ and $[K]$. Now consider a different but related eigenproblem:

$$\left([K]_{pq} - \lambda_b^a [M]_{pq}\right)^T \{\eta_b\} = 0 \tag{31}$$

Since the eigenvalues of a matrix are invariant with respect to the transpose operation [21:484], the eigenvalues from (31) will be the same as the eigenvalues from (29). However, the eigenvectors $\{\eta_b\}$ will not be the same as the eigenvectors $\{\phi_b\}$. Transposing (31) gives:

$$\{\eta_b\}^T \left([K]_{pq} - \lambda_b^a [M]_{pq}\right) = 0 \tag{32}$$

The eigenvector $\{\eta_b\}$ is called the *left eigenvector* because it pre-multiplies $\left([K]_{pq} - \lambda_b^a [M]_{pq}\right)$, whereas the standard *right eigenvector* post-multiplies $\left([K]_{pq} - \lambda_b^a [M]_{pq}\right)$.

Pre-multiplying (30) by $\{\eta_b\}^T$ gives:

$$\{\eta_b\}^T \left([K]_{pq} - \lambda_b^a [M]_{pq}\right) \frac{\partial \{\phi_b\}}{\partial \theta_j} + \{\eta_b\}^T \left(\frac{\partial [K]_{pq}}{\partial \theta_j} - \lambda_b^a \frac{\partial [M]_{pq}}{\partial \theta_j} - \frac{\partial \lambda_b^a}{\partial \theta_j} [M]_{pq}\right) \{\phi_b\} = 0 \tag{33}$$

The first term in (33) is equal to zero by (32). Solving for the antiresonance sensitivity gives:

$$\frac{\partial \lambda_b^a}{\partial \theta_j} = \frac{\{\eta_b\}^T \left(\frac{\partial [K]_{pq}}{\partial \theta_j} - \lambda_b^a \frac{\partial [M]_{pq}}{\partial \theta_j}\right) \{\phi_b\}}{\{\eta_b\}^T [M]_{pq} \{\phi_b\}} \tag{34}$$

Notice that if $[M]$ and $[K]$ are symmetric matrices, then $\{\eta_b\} = \{\phi_b\}$ and (34) reduces to the symmetric eigenvalue sensitivity equation (26). The sensitivities of $[K]_{pq}$ and $[M]_{pq}$ can be obtained by simply deleting row p and column q from the sensitivities of $[K]$ and$[M]$ from equations (27) and (28):

$$\frac{\partial [K]_{pq}}{\partial \theta_j} = \left[\frac{\partial [K]}{\partial \theta_j}\right]_{pq} \tag{35}$$

$$\frac{\partial [M]_{pq}}{\partial \theta_j} = \left[\frac{\partial [M]}{\partial \theta_j}\right]_{pq} \tag{36}$$

3.7 Mode Pairing

During the update process, the experimental eigenvalues and modeled eigenvalues must be paired in equations (12) and (20) so that they correspond to the same modes. An initial pairing can be made by a visual comparison of the mode shapes. However, as model parameters change during updating, modes may switch position in frequency. If left uncorrected such a switch could result in the erroneous pairing of, for example, a bending mode with a torsion mode. Therefore, some method of mode tracking must be used.

The Modal Assurance Criterion (MAC) was used to automatically pair mode shapes during updating. The MAC between an experimental eigenvector $\{\phi_e\}_j$ and a modeled eigenvector $\{\phi_m\}_k$ is defined as [9:57]:

$$MAC_{jk} = \frac{\left|\{\phi_e\}_j^T\{\phi_m\}_k\right|^2}{(\{\phi_e\}_j^T\{\phi_e\}_j)(\{\phi_m\}_k^T\{\phi_m\}_k)} \tag{37}$$

The MAC will have a value between 0 and 1 where 1 indicates an exact correlation. A MAC matrix can be formed by the MAC values for each combination of experimental and modeled mode shapes. The MATLAB^{TM} SDT function *ii_mac* was used to calculate the MAC matrix [3].

The mode shapes from the initial FE model were used to define the 11 "experimental" modes used in updating. The actual experimental mode shapes were not used because they were defined by only 8 DOF. The initial modeled mode shapes had 1488 DOF which provided a better MAC comparison between mode shapes during updating. The MAC matrix between the initial 11 mode shapes and the lowest 15 mode shapes calculated at some iteration in the update process (*iterative mode shapes*) was formed. Each iterative mode shape was paired to its maximum MAC value initial mode shape. If the maximum MAC value in a column of the MAC matrix was less than 0.7, the iterative eigenvalue corresponding to that iterative mode shape was removed from the update analysis.

Equations (23), (29), (37), (13), (12), (20), (21), (27), (28), (35), (36), (26), (34), (22), and (19) form the set of equations used in model updating. These equations are summarized in the context of the model updating process in Chapter 6.

Chapter 4 - Experimental Setup

The experimental setup did not change from previous AFIT research conducted by Captain Eric Swenson and Captain Richard Cobb. Therefore, this chapter includes only a brief description of the experimental setup. For more details see Swenson [37] and Cobb [5].

4.1 Flexible Truss Experiment

The FTE was originally part of the 12-Meter Truss Active Vibration Control Experiment developed for the Wright Laboratories Large Space Structures Technology Program [12]. The FTE was given to AFIT where it was set up as a vertically cantilevered 6-Meter truss. The assembled truss has a square cross section of 20 inches. It is made up of two equal length frames which are bolted together by horizontal plates at mid structure. Each of the two frames is made up of four vertical square cross section aluminum longerons that run the length of the frame. The longerons are connected by horizontal battens which divide the FTE into 8 bays. Each bay has four tubular bolt-in Lexan diagonal members arranged to create a back to back "K" pattern over the FTE. Figure 5 is a diagram of the FTE. For exact FTE dimensions see Swenson [37].

Although the FTE is called a truss, its connections are not pinned but bolted and welded, and can be more accurately described as a frame. The FTE diagonals are bolted to vertical plates which are welded to battens and longerons. These connections are called *vertical plate joints* and are shown in Figure 7. Two 3 meter frames are connected at the middle of the FTE by bolted horizontal plates that are welded to vertical plates and longerons. These joints are called the *mid-plate joints* and are shown in Figure 8. Horizontal plates are also present at the top of the FTE. These joints are called the *top-plate joints* and are shown in Figure 9. Finally, the locations where battens are welded to longerons, but no diagonals are present, are called the *regular batten joints*.

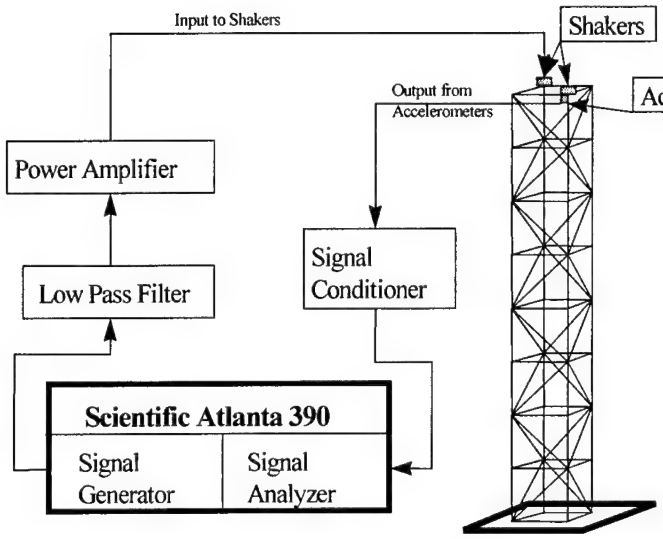

Figure 5. Diagram of Experiment Setup [37]

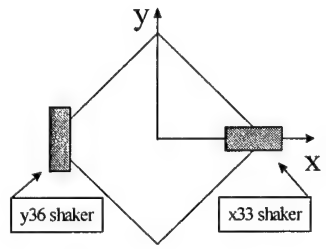

Figure 6. Top View of FTE

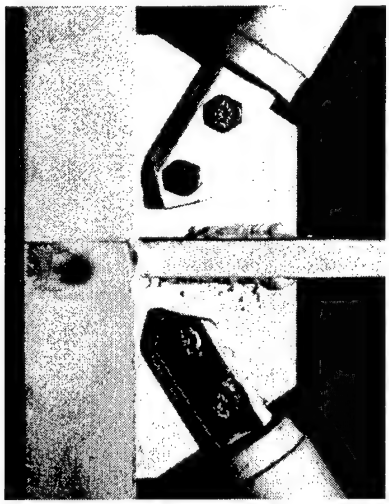

Figure 7. Vertical Plate Joint [37]

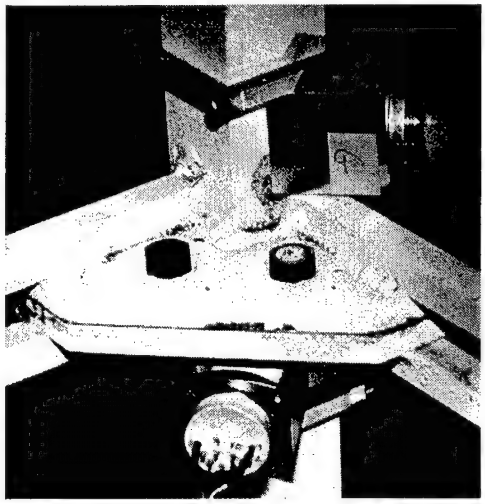

Figure 8. Mid-plate Joint [37]

The FTE lends itself easily to damage detection research. Removing diagonal members simulates a complete break of that member. Replacing a diagonal member with one with only 50% of the normal cross sectional area simulates a loss of stiffness in that member. For this research, 112 possible damage states and one undamaged state were considered. The 112 damage states consisted of 32 states where one diagonal was removed, 32 states where one diagonal had 50% the normal cross sectional area, and 48 combinations of two diagonals removed in the same bay.

4.2 Actuators and Sensors

The FTE is excited by two momentum exchange proof-mass actuators. The two actuators are named $x33$ and $y36$; because, in the FE model, they are positioned at node 33 and 36 and aligned in the x and y directions as shown in Figure 6. Each actuator contains a proof-mass that slides on low friction shafts. The proof-masses are centered by lightweight springs and accelerated by the electromagnetic field generated by coils fixed to the housing. Figure 9 shows one of the shakers. For the undamaged FTE, the $x33$ shaker primarily excites the x bending and breathing modes and the $y36$ shaker primarily excites the y bending and torsional modes.

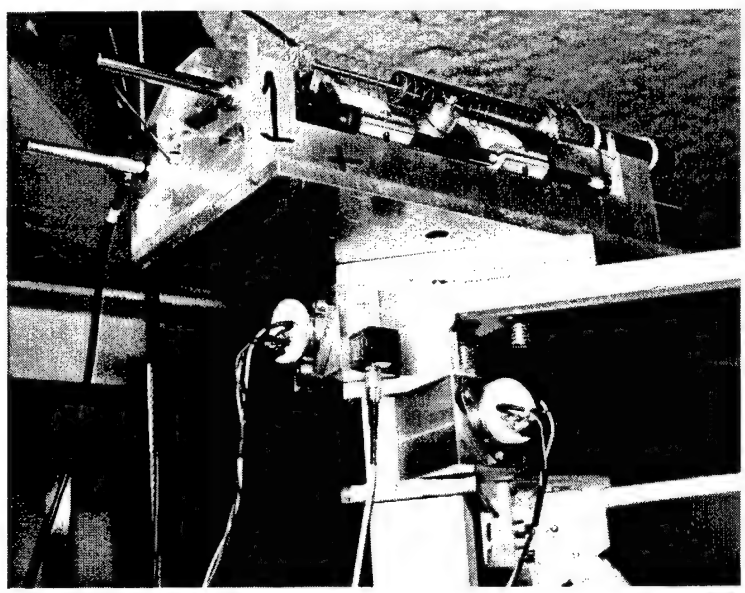

Figure 9. Shaker, Accelerometers, and Top-plate Joint [37]

Each shaker was used to generate a force input with an amplitude of approximately 1 pound peak to peak. The shakers produce 0.2 lbs per volt of periodic input signal. The two shakers were operated simultaneously from a common pseudo-random white noise voltage signal with an amplitude of 2.22 volts. The pseudo-random white noise was generated by the Scientific Atlanta Pro Series Dynamic Signal Analyzer (SA390) and cut off at 100 Hz by a low-pass filter.

Eight single-axis Sunstrand Q-Flex® accelerometers are bolted to the FTE, four at the mid section and four at the free end as shown in Figure 8 and Figure 9. The accelerometers are bolted

to the same two longerons as the shakers and aligned in the x and y directions. The accelerometer signals were amplified and conditioned before being sent to the SA390.

4.3 Data Collection

The SA 390 is a self contained Intel 486 personal computer (PC) with built-in digital signal processing boards. The SA 390 runs the Pro Series Analyzer acquisition software. The system is able to acquire, process, analyze, and display data from eight channels. The sampling rate for the SA 390 was set to 256 Hz. The SA 390 converted the amplified and conditioned accelerometer signals from analog to digital form. It then converted the time domain data into the frequency domain using a Fast Fourier Transform (FFT) algorithm. The input signal was multiplied by a Hanning window to prevent leakage. The FRF was computed by the SA 390 using the cross properties mode. The FRF, with range 0-100 Hz, consisted of 400 data points and was generated from 100 averaged FRFs, each generated from 1,024 time domain samples [35].

Eight measured FRFs, one from each accelerometer, were used in updating the FE model. These FRFs were recorded by averaging 2000 FRFs to ensure that they were very accurate. Two measured FRFs, one from each sensor collocated with a shaker, were used in damage detection. These FRFs were recorded by averaging 100 FRFs, which left some variability in the data but only took 18 seconds to accomplish. The experimental FRFs for all of the damaged configurations of the FTE were collected by Gaeta [11].

The SA 390 was controlled by an external program through the Dynamic Data Exchange (DDE) feature. The DDE allowed commands to be sent between MATLAB^{TM} and the Pro Series Analyzer software. Damage detection was initiated by executing a MATLAB^{TM} m-file that commanded the SA 390 to collect two FRFs from 100 averaged FRFs of the vibrating structure. The m-file then analyzed the returned measured FRFs to identify the damage state.

Chapter 5 - Finite Element Modeling

This chapter contains the development of the FE model of the FTE. A brief description of the FEM, the 12 DOF beam element, and the concept of differential stiffness is given. The FE model of the FTE is described along with the method of parameterizing the FTE joints. Lastly, the initial results from the model are given and compared to previous models of the FTE.

5.1 Finite Element Method

The FEM is a mathematical modeling technique that uses discrete point properties to model continuous structures. Elements are formed by placing modes along the boundaries of common shapes, describing the potential and kinetic energy of the body in terms of displacements at these nodes, and using these to form mass and stiffness matrices. Damping may also be incorporated in the system with damper elements or other methods. The equation of motion for the system is represented by the second-order matrix differential equation in equation (38).

$$[M]\{\ddot{d}\} + [C]\{\dot{d}\} + [K]\{d\} = \{f\} \tag{38}$$

where

$[M]$ = mass matrix

$[C]$ = damping matrix

$[K]$ = stiffness matrix

$\{d\}$ = displacement vector

$\{f\}$ = force vector

$\{\dot{d}\}$ and $\{\ddot{d}\}$ = first and second time derivatives of $\{d\}$

If $[C]$ is proportional to $[M]$ and $[K]$ then equation (38) can be uncoupled by a coordinate transformation to modal coordinates. This coordinate transformation involves the use of the system modal matrix $[\phi]$, whose columns are the eigenvectors of equation (38) with $[C] = [0]$. The FEM equation of motion can be transformed to modal coordinates in a two step process: 1) Let

$\{d\} = [\phi]\{q\}$, 2) Pre-multiply by $[\phi]^T$. If $[\phi]$ is normalized such that $[\phi]^T[M][\phi] = [I]$, where $[I]$ is the identity matrix (this is called mass normalization), the modal FEM equation of motion is [21:195]:

$$\{\ddot{q}\} + [2\zeta\omega_n]\{\dot{q}\} + [\omega_n^2]\{q\} = \{p\} \tag{39}$$

where

$[\omega_n^2] = [\phi]^T[K][\phi]$ = a diagonal matrix of natural frequencies squared

$[2\zeta\omega_n] = [\phi]^T[C][\phi]$ = a diagonal matrix of damping factors multiplied by $2\omega_n$

$\{p\} = [\phi]^T\{f\}$ = modal force vector

$\{q\} = [\phi]\{d\}$ = modal displacement vector

This is often the easiest form of the equations for determination of forced response.

5.2 Finite Elements Used

The Structural Dynamics Toolbox^{TM} (SDT) for MATLAB^{TM} was used to create a FE model of the FTE. The SDT beam element, *beam1*, was used to model all the members of the FTE. The beam1 element is the standard 12 DOF beam element, with 3 translational and 3 rotational DOF at each of its 2 nodes. A diagram of the element DOF is included in Figure 10. (Note that the 12 DOF beam element does not use a right handed coordinate system. This is consistent with the definition of the element used in the SDT.) The SDT uses consistent mass matrices for the elemental mass matrices. The elemental stiffness matrices use linear interpolations for beam traction and torsion and cubic interpolations for flexion. The mass and stiffness matrices for the beam1 element are included in Appendix A along with the geometric and material properties of the FTE members.

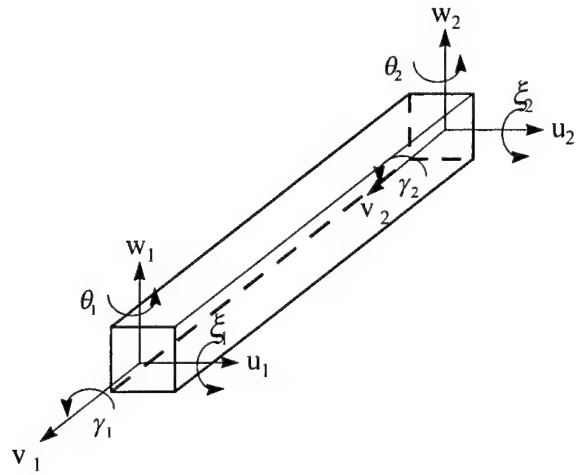

Figure 10. 12 DOF Beam Element [37]

Coordinate transformations were applied to the element matrices of Appendix A to rotate the elements into their positions in 3D space. The element matrices were then assembled in order to create the global mass and stiffness matrices of equation (38). For a more thorough development of the FEM, the derivation of beam elements, consistent mass, or global matrix assembly, refer to any FE text, e.g. [6].

5.3 Non-Linear Stress Softening

The SDT beam1 element consists of independent axial and flexural stiffnesses. However, axial loads and bending deformations can be coupled through a second order effect that is normally ignored in strictly linear FEM theory. The second order effect is often called differential stiffness and will be explained by way of example.

Consider the beam under the distributed load q in Figure 11a. The beam undergoes a bending deformation of magnitude w_c at the beam midpoint. The beam in Figure 11b is under an axial load P and a distributed transverse load q. The bending deformation, caused by q, attempts to draw the beam endpoints in toward the center, but the axial load P pulls the beam ends in the opposite directions. Clearly, the presence of the axial load P reduces the amount of bending deformation.

Therefore, a beam under axial tension is said to be *stress stiffened.* Similarly, axial compression increases the amount of bending deformation and softens the beam.

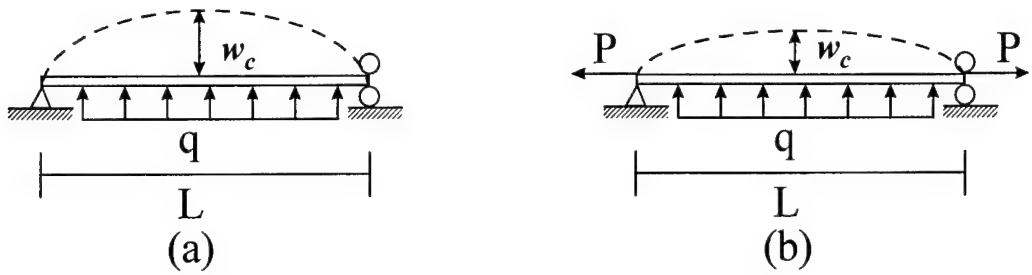

Figure 11. Non-linear Stress Stiffening in Beams

The standard beam elemental stiffness matrix can be easily corrected to account for stress stiffening or softening by adding the following corrective stiffness matrix [6:434]:

$$[k_\sigma] = \frac{P}{30L}\begin{bmatrix} 36 & -3L & -36 & -3L \\ -3L & 4L^2 & 3L & -L^2 \\ -36 & 3L & 36 & 3L \\ -3L & -L^2 & 3L & 4L^2 \end{bmatrix} \tag{40}$$

with nodal DOF $\{d\} = \begin{bmatrix} w_1 & \xi_1 & w_2 & \xi_2 \end{bmatrix}^T$ as shown in Figure 10. By including the same corrective stiffness matrix for the nodal DOF $\{d\} = \begin{bmatrix} u_1 & \theta_1 & u_2 & \theta_2 \end{bmatrix}^T$, and by inserting the appropriate rows and columns of zeros for the other DOF, the corrective stiffness matrix was expanded to a 12 by 12 matrix and added to the element stiffness matrix.

This thesis included non-linear stress softening in the FE analysis because Cobb's, Swenson's, and this research's FE updates all greatly reduced the elastic modulus of the longerons. The longeron elastic modulus was reduced by as much as 30%, which indicated a large modeling error in that parameter. It was thought that ignoring stress softening may have been one cause of the modeling error in longeron stiffness, since the longerons were long (6 meters), thin-walled (0.065 inches), and under a 7.5 lbs compressive static load from each shaker. However, stress softening had a very small effect on the FE model. The first bending mode had the largest change when stress softening was included. It was reduced in natural frequency by only 0.07%.

In this research, the element axial loads, P in equation (40), were determined by a static solution of FTE under the load of its own weight. The NASTRAN^{TM} function GRAV [32:616] was used to generate nodal loads based on the FE model mass matrix. The internal beam forces were output from NASTRAN^{TM} and input into the SDT model. As expected, the static load of the FTE was almost entirely carried by the vertically oriented longerons, and the diagonals and battens were nearly zero-force members. The SDT beam1 element was modified to accept the axial load P from the NASTRAN^{TM} static solution, form $[k_\sigma]$, and add it to the standard beam stiffness matrix before coordinate transformations are applied.

5.4 Joint Model

The FE model created for this research, called the *joint model*, sought to incorporate the positive attributes of both Cobb's baseline model and Swenson's stiff model. The joint model would model the FTE joints and place the diagonal end masses in realistic locations as in Swenson's model. It would also use few DOF as in Cobb's model. In addition, the joint model added the new feature of using the joint dimensions as update parameters.

The vertical plate joints were modeled using rigid links as shown in Figure 12. One rigid link was used to place the lumped diagonal end mass in its realistic position. Another rigid link was used to connect to the diagonal beam element to the master node. This rigid link could be shorter than the distance to the lumped mass so that the joint would not be overstiffened. The regular batten, mid-plate and top-plate joints were modeled similarly as shown in Figures 13, 14, and 15. The distances in Figures 12, 13, 14, and 15 (d_L, d_M, d_B, d_K, d_{RB}, d_{MP}, d_{TP}) represent the lengths of the rigid links that were used to parameterize the joint. The subscripts L, M, B, K, RB, MB and TP stand for *Longeron*, *Mass*, *Batten*, *Stiffness*, *Regular Batten*, *Mid-Plate*, and *Top-Plate*.

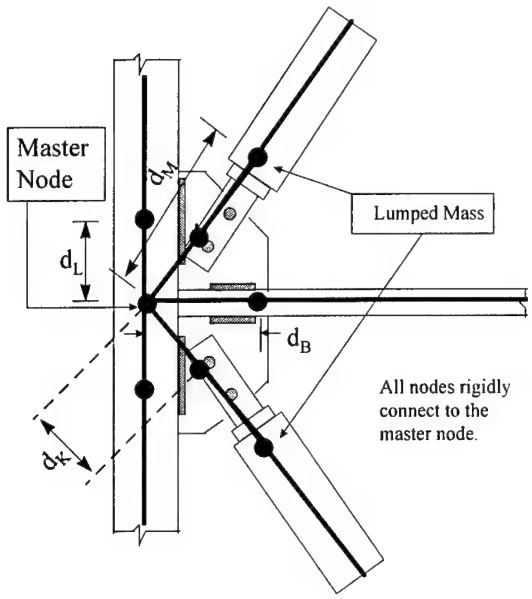

Figure 12. Vertical Plate Joint FE Mesh

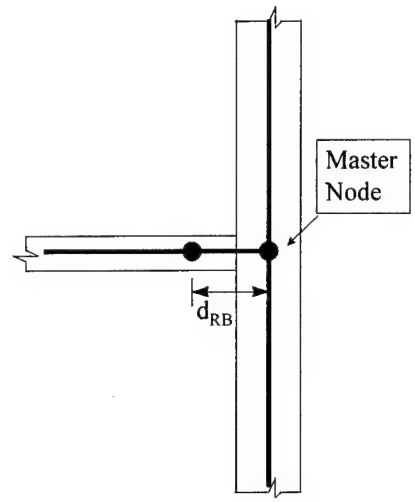

Figure 13. Regular Batten Joint FE Mesh

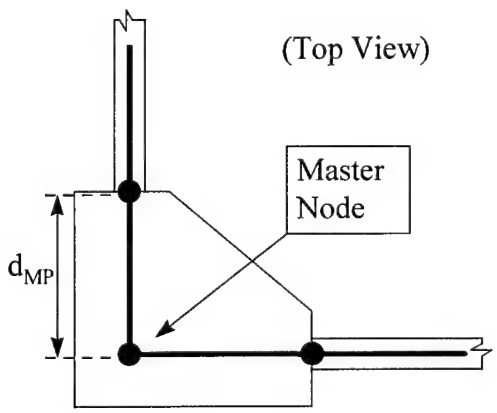

Figure 14. Mid-plate Joint FE Mesh

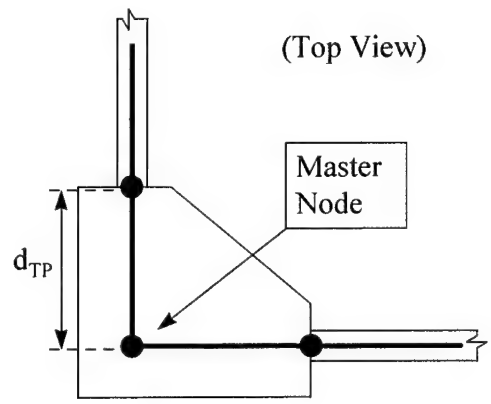

Figure 15. Top-plate Joint FE Mesh

The joint model had several other improvements over previous models. Each proof mass actuator was modeled as a lumped mass with no mass in the actuated DOF. This reflected the near frictionless sliding of the proof mass along one axis. The actuator masses were offset above the top of the FTE by 2.5 inches and the top sensors were offset below the top of the FTE by 2 inches to reflect their real positions. Again, this was accomplished using rigid links. Lastly, since the rigid links lengthened and shortened the beam elements from their realistic lengths, additional lumped masses were placed at the endpoints of the beam elements to maintain correct mass during

updating. The amount of these additional masses varied to correct for the amount of mass added or lost by changes in beam element length. The accelerometers, bolts, and welds in the FTE were also modeled as lumped masses.

The joint model used 248 nodes but only had 192 DOF, the same size as Cobb's baseline model. Each node that was attached by a rigid link had no DOF of its own, because it was slaved to a master node through a coordinate transformation matrix [6:220]. This made rigid links a very efficient way to parameterize joints. The SDT was used to assemble the global FE mass and stiffness matrices, reduce out rigid DOF, solve for the first 20 normal modes, and plot the FRFs for the 8 accelerometers. The whole process required 23 seconds on a 166 MHz Pentium PC.

5.5 Initial Model Results

Initial values were chosen for the joint parameters based on the geometry of the joints. Table 2 shows the initial values used for the joint parameters. As mentioned previously, the longerons were found to be too stiff in the model. This was the reason for including non-linear stress softening correction elements in the analysis. The longerons certainly should not be stiffened further by rigid links in their joints, and therefore d_L was made effectively zero.

Table 2. Initial Joint Parameters

Joint Parameter See Figures 12, 13, 14, and 15 for Parameter Definitions	Inital Value (Inches)
d_L	0.1
d_M	4.5
d_B	1.0
d_K	2.0
d_{RB}	0.5
d_{MP}	2.5
d_{TP}	2.5

Using the parameters from Table 2, the initial fit between the joint model FRFs and the experimental FRFs are shown in Figure 16. Modal damping of 0.01 was applied to all FE model modes for plotting appearance only.

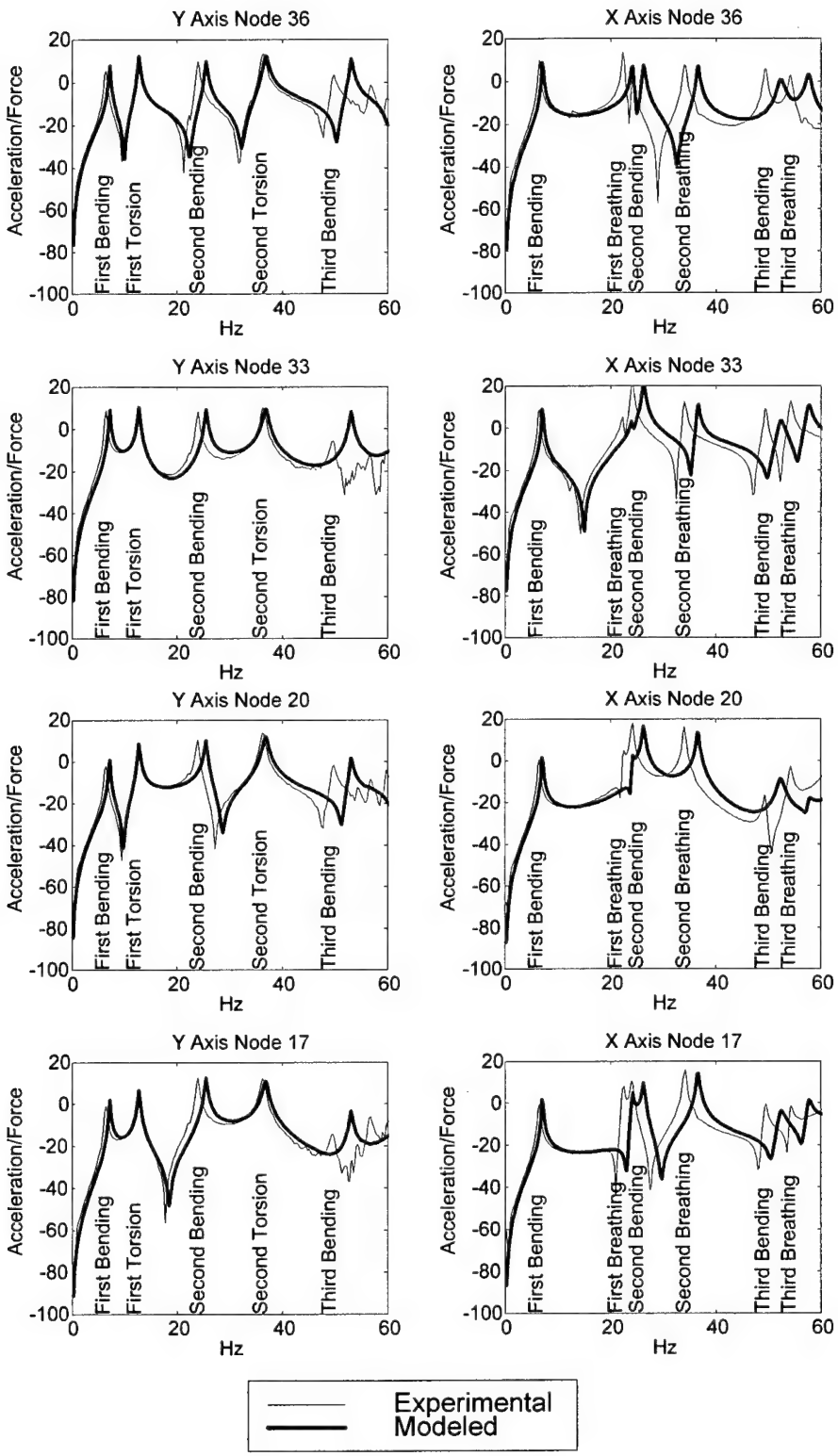

Figure 16. Joint Model FRFs Before Updating

During the development of the joint model, emphasis was placed on obtaining the correct order of resonances and antiresonances in the FRFs. It was especially difficult to get an antiresonance to appear between the first breathing and second bending modes in the x36 FRF (See Figures 1, 2, 3 and 4). In fact, as part of this research many parameters in Cobb's and Swenson's models were varied in an attempt to correctly model the x36 antiresonance between the first breathing and second bending modes. These models never produced such an antiresonance even after updating. The apparent inability of these models to correctly order the resonances and antiresonances indicated a systematic modeling error that consistently produced mode shapes for which the products $\{\phi_{1st\ breathing}\}_{x36}\{\phi_{1st\ breathing}\}_{x33}$ and $\{\phi_{2nd\ bending}\}_{x36}\{\phi_{2nd\ bending}\}_{x33}$ were not the same sign (See equation (2)). An antiresonance can only appear between the first bending and second breathing modes if these two products are of the same sign, so that the response at the measured DOF due to the first mode destructively interferes with the response at the measured DOF due to the second.

In creating the joint model, it was found that modeling the regular batten joints with rigid links (Figure 13) and removing the proof mass actuator mass in the direction of actuation were the critical modeling changes that produced the correct resonance-antiresonance order in the x36 FRF. A comparison of the first breathing and second bending mode shapes from the stiff model and the joint model is shown in Figure 17. Clearly, re-ordering the resonances and antiresonances to match experimental data forced changes in the mode shapes. Figure 17 provides another motivating illustration for using antiresonances as an indirect way to update mode shapes in FE models.

The initial FE model showed the correct order resonances and antiresonances in all 8 FRFs. Therefore, this model was chosen as the starting point for model updating using natural frequencies and antiresonant frequencies. Model updating is covered in the next chapter.

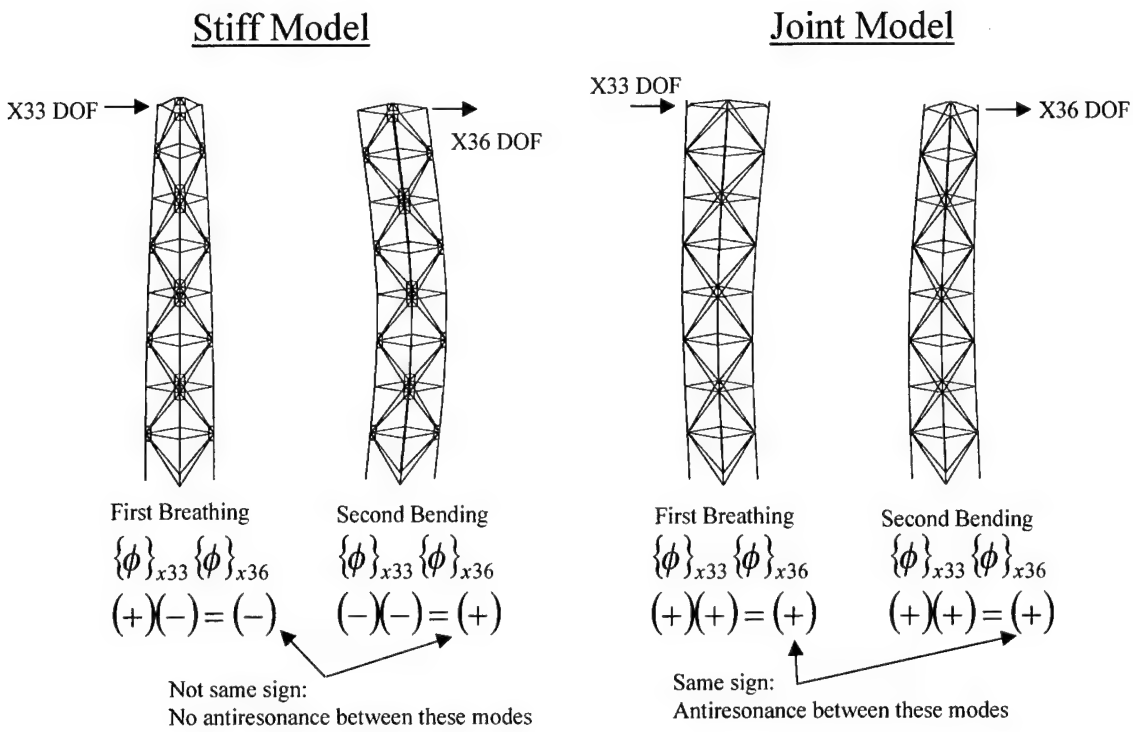

Figure 17. Mode Shape Comparison Between Stiff and Joint Models

Chapter 6 - Finite Element Model Updating

This chapter describes the process and results of FE model updating on the FTE. An overview of the iterative update process is presented with the equations required in updating. The identification of natural frequencies and antiresonant frequencies is discussed. The reasons for the choices of update parameters and weighting matrices are given. Finally, the results are compared for two model updates. The first used antiresonant frequencies and natural frequencies and the second used only natural frequencies.

6.1 Introduction

There were several motivations for using antiresonant frequencies to update the FE model of the FTE. Previous models of the FTE had produced reasonable correlations between model and experimental data in terms of overall FRFs or natural frequencies. However, these models produced a poor correlation between modeled and experimental antiresonances (see Figures 2 and 4). Therefore, it was anticipated that the use of antiresonances in updating would improve existing models. Also, previous research had produced better damage detection results with modal updated models than with FRF updated models (see Table 1). Antiresonances again seemed attractive, because they can be derived as modal parameters of submatrices of the system matrices (see equation (11)). Lastly, researchers such as Lallement [19], Rade [30], Mottershead [25], and Friswell [9] have recently shown that the use of antiresonance in model updating increases the knowledge space, serves as a more accurate substitute for mode shape data, and can improve update results.

6.2 Overview

The joint model required updating to improve its fit to the experimental FRFs. The approach taken in matching the experimental and modeled FRFs was to match the experimental and modeled natural frequencies and antiresonant frequencies. The penalty method was chosen as the update

method, because it accommodated the use of antiresonant frequencies in updating and the use of a wide variety of possible update parameters. Since most of the errors in the FE model were assumed to be in the modeling of the joints, the lengths of the rigid links that model the joints were used as update parameters. Figure 18 shows the process of model updating.

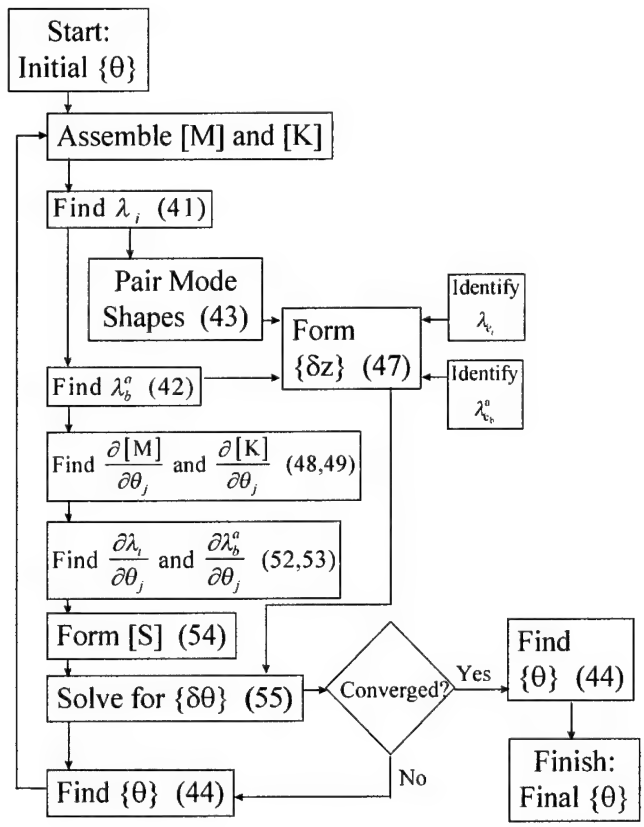

Figure 18. FE Update Method Flowchart

The equations used in FE model updating were developed in Chapter 3 and are repeated here for convenience.

$$([K] - \lambda_i [M]) \{\phi_i\} = 0 \tag{41}$$

$$\left([K]_{pq} - \lambda_b^a [M]_{pq}\right) \{\phi_b\} = 0 \tag{42}$$

$$MAC_{jk} = \frac{\left|\{\phi_e\}_j^T \{\phi_m\}_k\right|^2}{(\{\phi_e\}_j^T \{\phi_e\}_j)(\{\phi_m\}_k^T \{\phi_m\}_k)} \tag{43}$$

$$\delta\theta_j = \theta_{new_j} - \theta_{old_j} \qquad j = 1 \ldots r \tag{44}$$

$$\delta z_i = \lambda_{e_i} - \lambda_{m_i} \qquad i = 1 \ldots n \tag{45}$$

$$\delta z_b^a = \lambda_{e_b}^a - \lambda_{m_b}^a \qquad b = 1 \ldots k \tag{46}$$

$$\{\delta z\}^* = \left\{ \begin{array}{c} \{\delta z\}_{nx1} \\ \{\delta z^a\}_{kx1} \end{array} \right\} \tag{47}$$

$$\frac{\partial [K]}{\partial \theta_j} \approx \frac{\left[K\left(\theta_{0_j} + \delta\theta_j\right)\right] - \left[K\left(\theta_{0_j}\right)\right]}{\delta\theta_j} \tag{48}$$

$$\frac{\partial [M]}{\partial \theta_j} \approx \frac{\left[M\left(\theta_{0_j} + \delta\theta_j\right)\right] - \left[M\left(\theta_{0_j}\right)\right]}{\delta\theta_j} \tag{49}$$

$$\frac{\partial [K]_{pq}}{\partial \theta_j} = \left[\frac{\partial [K]}{\partial \theta_j}\right]_{pq} \tag{50}$$

$$\frac{\partial [M]_{pq}}{\partial \theta_j} = \left[\frac{\partial [M]}{\partial \theta_j}\right]_{pq} \tag{51}$$

$$\frac{\partial \lambda_i}{\partial \theta_j} = \frac{\{\phi_i\}^T \left(\frac{\partial [K]}{\partial \theta_j} - \lambda_i \frac{\partial [M]}{\partial \theta_j}\right) \{\phi_i\}}{\{\phi_i\}^T [M] \{\phi_i\}} \tag{52}$$

$$\frac{\partial \lambda_b^a}{\partial \theta_j} = \frac{\{\eta_b\}^T \left(\frac{\partial [K]_{pq}}{\partial \theta_j} - \lambda_b^a \frac{\partial [M]_{pq}}{\partial \theta_j}\right) \{\phi_b\}}{\{\eta_b\}^T [M]_{pq} \{\phi_b\}} \tag{53}$$

$$[S]^* = \begin{bmatrix} \frac{\partial \lambda_1}{\partial \theta_1} & \cdots & \frac{\partial \lambda_1}{\partial \theta_r} \\ \vdots & \ddots & \vdots \\ \frac{\partial \lambda_n}{\partial \theta_1} & \cdots & \frac{\partial \lambda_n}{\partial \theta_r} \\ \frac{\partial \lambda_1^a}{\partial \theta_1} & \cdots & \frac{\partial \lambda_1^a}{\partial \theta_r} \\ \vdots & \ddots & \vdots \\ \frac{\partial \lambda_k^a}{\partial \theta_1} & \cdots & \frac{\partial \lambda_k^a}{\partial \theta_r} \end{bmatrix} \tag{54}$$

$$\{\delta\theta\} = \left[[S]^{*T} [W_{\varepsilon\varepsilon}] [S]^* + [W_{\theta\theta}]\right]^{-1} \left\{[S]^{*T} [W_{\varepsilon\varepsilon}] \{\delta z\} - [W_{\theta\theta}] \{\{\theta\} - \{\theta\}_0\}\right\} \tag{55}$$

6.3 Eigenvalue and Antiresonance Identification

The first step in model updating was to identify the experimental eigenvalues and antiresonant eigenvalues. This process is indicated by the two boxes labeled *identify* in Figure 18. Eigenstructure realization algorithm (ERA) was chosen as the modal identification technique for this research because of its accuracy in identifying closely space modes, and its ability to work with MIMO systems. ERA uses time domain impulse response functions, which are found via an inverse Fourier Transform of the FRFs, to construct a state space model of the system. It then identifies the modal parameters by completing an eigensolution of the state space system matrix [16]. Since ERA produces extraneous computational modes, the extended modal amplitude coherence (EMAC) was used as a measure of confidence that the identified mode was present in the experimental structure. An EMAC of 100% indicated a perfect correspondence between the identified mode and the experimental mode.

A MIMO ERA MATLAB^{TM} m-file written by Dr. Joseph Hollkamp was used to identify the natural frequencies of the FTE. The natural frequencies and corresponding EMACs are included in Table 3. All but one mode was identified with EMACs above 90% which indicated a successful modal identification. Results closely matched the location of the resonant peaks in the experimental FRFs as expected.

Table 3. Identified Natural Frequencies

Mode	Natural Frequency (Hz)	EMAC (%)
1st Bending - x	6.40	98.02
1st Bending - y	6.43	98.68
1st Torsion	12.69	96.54
1st Breathing	22.33	97.63
2nd Bending - x	24.22	99.18
2nd Bending - y	24.03	98.65
2nd Torsion	36.42	98.05
2nd Breathing	34.14	99.18
3rd Bending - x	49.58	83.09
3rd Bending - y	49.68	98.85
3rd Breathing	54.47	92.84

For this lightly damped structure, the antiresonant natural frequencies were assumed to be very near the antiresonant frequencies. Therefore, the antiresonant frequencies were visually taken from the experimental FRFs using the MATLAB^{TM} *zoom* function. The 21 identified antiresonant frequencies used in updating are marked with x's in Figure 19. An algorithm for the automatic identification of antiresonant frequencies from experimental FRFs warrants further research.

The identified natural frequencies and antiresonant frequencies were all squared and formed into a vector. The difference between this vector and its FEM counterpart was used to form the $\{\delta z\}$ in Figure 18 according to equations (45), (46), and (47).

6.4 Choice of Update Parameters

The choice of update parameters is critical to successful model updating. Update parameters should represent areas of the model where modeling errors are likely. Also, the measurements used in updating (natural frequencies and antiresonant frequencies in this research) should be sensitive to the update parameters chosen. Update parameters that have a similar effect on the modal data, such as the length of a beam and its flexural rigidity, should be avoided. Lastly, the number of update parameters should be as few as possible to keep the problem well conditioned. These guidelines help make the update process fast, stable, unique, and physically meaningful [9:279].

For the FTE, the likely source of modeling error was in the joints. Therefore, five parameters were chosen to be the joint rigid link parameters d_K, d_B, d_{RB}, d_{TP}, and d_{MP} as defined in Figures 13, 14, and 15. The longeron elastic modulus (E_L) was included as a global update parameter which could affect all modes. E_L was also included because previous model updates had required large reductions in E_L to lower the bending modes to match experimental data. The longeron rigid link d_L was left at its initial value of 0.1, because any increase in rigid length d_L would force a greater reduction in E_L to compensate.

Trial updates with these parameters resulted in convergence to negative values for d_B and d_{RB}. Although physically unrealistic, the negative values indicated that the update algorithm

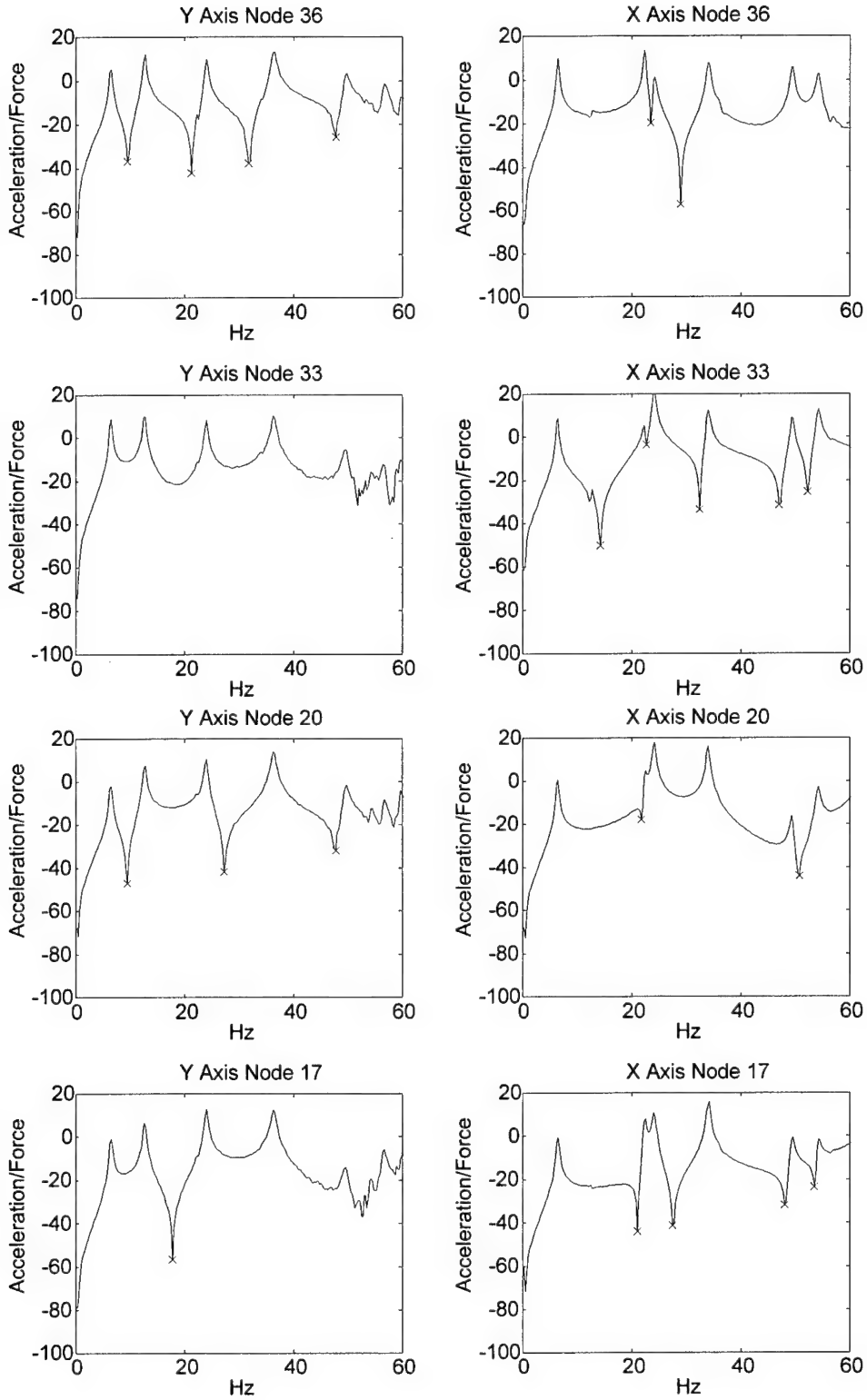

Figure 19. Identified Antiresonant Frequencies Used in Updating

desired to reduce the flexural rigidity of the battens by increasing batten length. Therefore, the battens' bending moment of inertia (I_{batt}) was included as another parameter so that the algorithm could reduce the flexural rigidity of the battens directly without having to use negative joint dimensions to increase batten lengths. The final set of update parameters is shown in Table 5.

Update parameters must be scaled so that a perturbation in each one produces eigenvalue and antiresonance sensitivities of similar magnitude. This is necessary for the update method to be well conditioned. The parameters E_L and I_{batt} were scaled so that their initial values were one. The rigid link dimensions in inches were used for the joint parameters without any scaling.

6.5 Choice of Weighting Matrices

Another strength of the penalty method is the ability to assign weighting matrices to both the measured data and the parameter estimates (See equation (19)). The weighting matrix $[W_{\varepsilon\varepsilon}]$ was included in the model updating algorithm to account for different levels of error in the different measurements. For example, natural frequencies are typically measured more accurately than mode shapes. The weighting matrix $[W_{\theta\theta}]$ was included in the model updating algorithm in order to account for the different ranges on the parameters. For example, it may be desired to allow relatively large changes to one parameter and relatively small changes to another. Friswell and Mottershead recommend letting the weighting matrices $[W_{\varepsilon\varepsilon}]$ and $[W_{\theta\theta}]$ be diagonal matrices with their elements equal to the reciprocal of the corresponding estimated measurement and parameter variances [9]. The variance is calculated as the standard deviation squared. The estimated standard deviations are chosen based on an assumption that each measurement or parameter is one sample from a statistical distribution of possible measurements and parameters [23:362].

The standard deviations of the natural frequencies were assumed to be 0.5% of their identified values. The standard deviations of the antiresonant natural frequencies were assumed to be 1% of their identified values since they were obtained visually. The standard deviations of the update parameters were based on the reasonable limits of rigid joint dimensions and thereby on

the geometry of the FTE joints. The estimated standard deviations of the update parameters are included in Table 4. The standard deviations were squared to get the variances, inverted, and placed on the diagonals of the weighting matrices.

Table 4. Estimated Standard Deviations of the Update Parameters

Update Parameter	Estimated Standard Deviation
E_L	10%
I_{batt}	10%
d_K	1.00 inch
d_B	0.50 inch
d_{RB}	0.25 inch
d_{TP}	0.50 inch
d_{MP}	0.50 inch

6.6 Updating Results

The first update, called the antiresonant update because it included antiresonance data, converged in five iterations taking 19.5 minutes on a 166 MHz Pentium PC. Convergence was defined as the Euclidean norm of the parameter step vector $\{\delta\theta\}$ being less than 0.01. Updating results are shown in Table 5. The final joint parameters satisfied physical intuition. The mid-plate joint was slightly more rigid than the top-plate joint, because it was made of two horizontal plates instead of one. The batten rigid link was twice as long as the regular batten rigid link, because the battens were not welded to vertical plates in the regular batten longeron joint. All the rigid link dimensions remained physically reasonable based on the joint geometries. The update made large changes in the parameters E_L and I_{batt}. The physical reason for the large amount of model error in these variables is unknown. Perhaps both the longerons and battens have a varying wall thickness that is thinner than the wall thickness used in the model. However, when wall thicknesses were used as update parameters the resulting model produced worse results.

Table 5. Final Parameter Values from Antiresonant Update

Update Parameter	Initial Value	Iteration 1	Iteration 2	Iteration 3	Iteration 4	Final Value
E_L	1.0	0.6871	0.7092	0.7098	0.7098	0.7098
I_{batt}	1.0	0.6787	0.5654	0.5966	0.5982	0.5982
d_K	2.0	1.7150	1.8976	1.8968	1.8967	1.8967
d_B	1.0	0.6734	1.0596	0.8822	0.8738	0.8741
d_{RB}	0.5	0.3241	0.5085	0.4251	0.4284	0.4287
d_{TP}	2.5	3.2060	3.7164	3.6144	3.6102	3.6102
d_{MP}	2.5	3.2152	3.7443	3.6367	3.6319	3.6318

In order to evaluate the benefit of using antiresonance data in updating, another update, called the *non-antiresonant update*, with the same update parameters, starting point, and convergence criteria was accomplished using only the identified natural frequencies in Table 3. Thus the sensitivity matrix $[S]$ in equation (54) was reduced from a 32 x 7 matrix to an 11 by 7 matrix. The update was initially unstable. The weighting matrix on the initial parameters, $[W_{\theta\theta}]$ in equation (55), had to be multiplied by 30 to get the update to converge on a set of final values for the update parameters. The instability was expected based on the fact that the update was solving for the same number of unknown parameters with fewer equations. The update converged in 4 iterations and required 5.7 minutes of computation on a 166 MHz Pentium PC. The results of the update is shown in Table 6. The final non-antiresonant update parameters changed less from their initial values than in the antiresonant update, which was expected because $[W_{\theta\theta}]$ was 30 times greater.

Table 6. Final Update Parameter Values from Non-Antiresonant Update

Update Parameter	Initial Value	Iteration 1	Iteration 2	Iteration 3	Final Value
E_L	1.0	0.7098	0.7235	0.7235	0.7235
I_{batt}	1.0	0.9038	0.8917	0.8886	0.8879
d_K	2.0	1.6396	1.7833	1.7855	1.7877
d_B	1.0	0.8474	0.8579	0.8649	0.8660
d_{RB}	0.5	0.4535	0.4594	0.4623	0.4628
d_{TP}	2.5	2.1482	2.1555	2.1677	2.1688
d_{MP}	2.5	2.3868	2.4065	2.4162	2.4180

Figures 20 and 21 show the FRFs from the antiresonant and non-antiresonant updated joint models. Modal damping of 0.01 was applied to all FE model modes for plotting appearance

only. Both updated joint models visibly match the experimental data better than previous updated models (see Figures 2 and 4).

Table 7 compares the non-updated, the non-antiresonant updated, and the antiresonant updated joint models in Figures 16, 20 and 21 to experimental data based on the following cost function:

$$J = \sum \left(\log \left| [H(\omega)]_{Experimental} \right| - \log \left| [H(\omega)]_{modeled} \right| \right)^2 \tag{56}$$

where $[H(\omega)]$ is a matrix whose columns are the 8 complex valued FRFs from the 8 FTE accelerometers. Each FRF consisted of 240 frequency points spaced evenly between 0 and 60 Hz.

Table 7. Cost Function Values Before and After Updating

FE Model	Cost Function Value
Non-Updated Joint Model	69.14
Non-Antiresonant Updated Joint Model	12.27
Antiresonant Updated Joint Model	6.59

Based on Table 7, the antiresonant updated joint model produced a 46% better correlation to the experimental FRFs than the non-antiresonant updated joint model. The antiresonant updated joint model especially outperformed the non-antiresonant updated model in the troublesome region around the first breathing and second bending modes of the x36 FRF (see Figures 21 and 20). Model updating using antiresonant frequencies was successful at modeling the undamaged FTE. The next chapter examines whether or not antiresonance updating produced a physically realistic model.

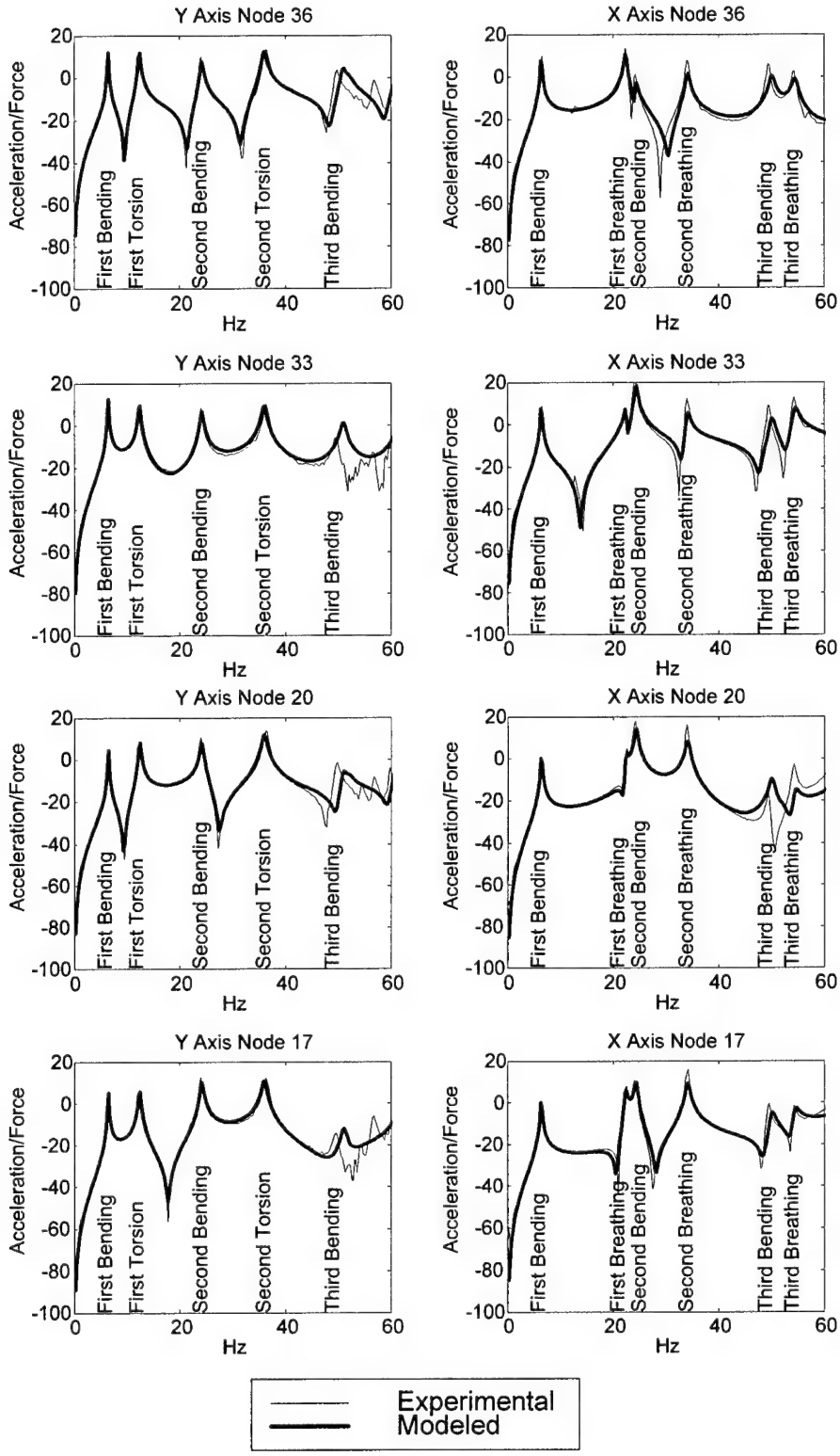

Figure 20. Non-Antiresonant Updated Joint Model FRFs

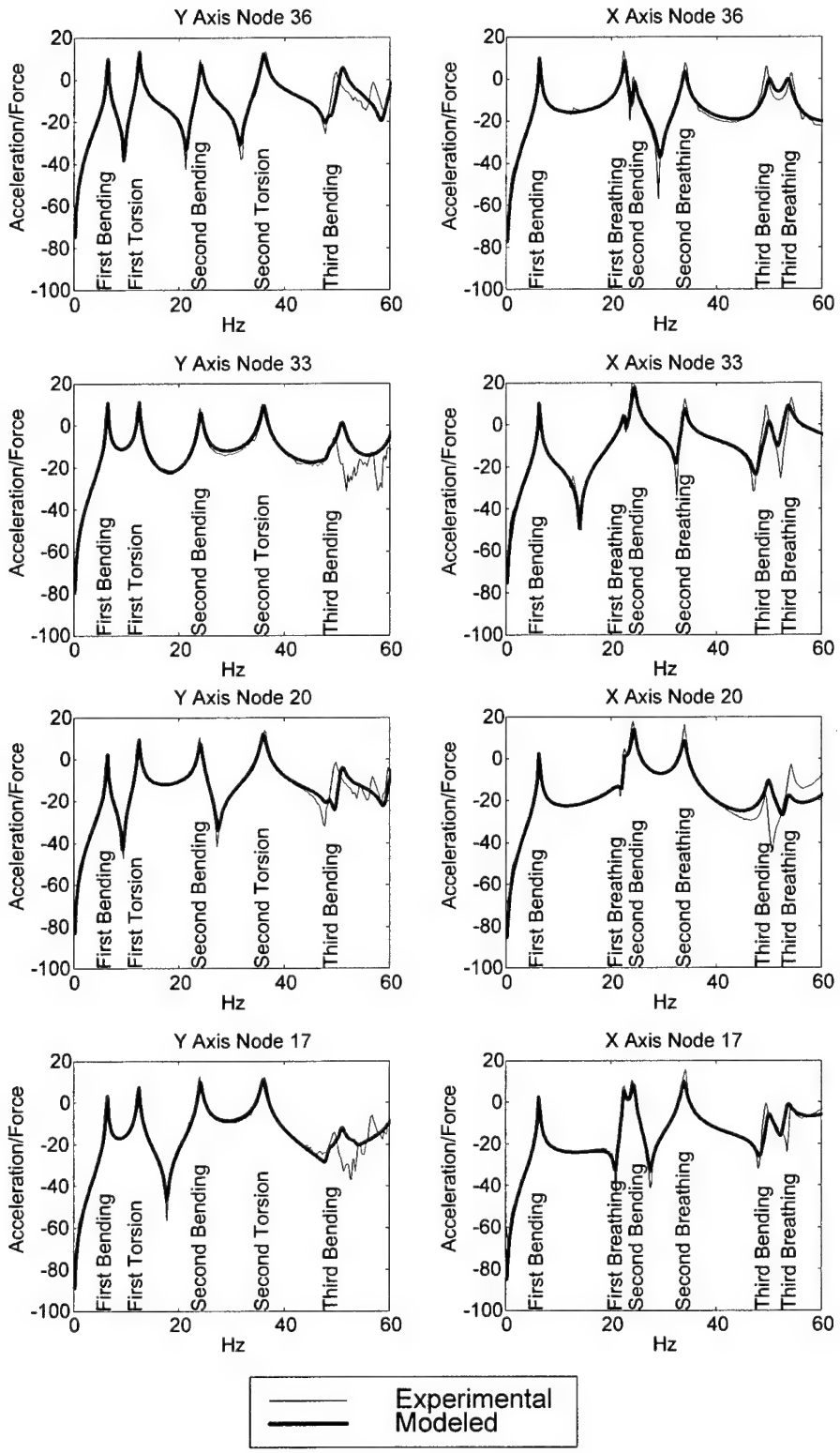

Figure 21. Antiresonant Updated Joint Model FRFs

Chapter 7 - Damage Detection

This chapter describes the process and results of damage detection on the FTE. A description of the 112 damaged configurations of the FTE is given. A pattern classifier and a curve-fit method of damage detection are described and applied to the damaged FTE configurations. Damage detection results from both methods are presented and compared to previous damage detection efforts on the FTE.

7.1 Introduction

An updated model may match the experimental data used in updating without matching other experimental data not used in updating, such as the response at higher frequencies, other sensor locations, or the responses under different structural configurations, boundary conditions, or loadings. Such an updated model is not physically realistic, and the updated parameters do not necessarily correct modeling errors. The true test of a FE update method is whether the updated parameters corrected modeling errors and resulted in a more physically realistic model.

For this research, the physical correctness of the antiresonant updated joint model was validated by using the model to predict the FRFs of damaged configurations of the FTE. The modeled FRFs were compared to the experimental FRFs using two damage detection methods - a pattern classification method and a curve-fit method.

7.2 Flexible Truss Experiment Damage

A total of 112 possible damaged configurations of the FTE were considered. The first 32 damage cases corresponded to configurations where a single bolt-in diagonal was removed from the FTE. Cases where a diagonal was completely removed were called *100% damage cases*. Another 32 damage cases corresponded to configurations where a single bolt-in diagonal was replaced with a diagonal that had only 50% of the normal cross sectional area. The 50% diagonal was created by cutting a diagonal in half length-wise. These cases were called *50% damage*

cases. Lastly, 48 damage cases corresponded to configurations where two diagonals were removed simultaneously from a single bay of the FTE. These cases were called *double damage cases*.

The FTE damage cases were modeled using the antiresonant updated joint model. The 100% damage cases were modeled by deleting a diagonal element and its lumped end masses in the FE model. The 50% diagonal cases were modeled by a diagonal element with 50% the normal cross sectional area and recalculated bending moments of inertia (I_1 and I_2). Tracking the modal damping for each mode was not feasible, because, in damaged configurations, modes switched positions and new modes shifted down into the 0 to 60 Hz frequency range of interest. Therefore, modal damping of 0.01 was applied to all FE model modes.

Only the two sensors collocated with the actuators, x33 and y36, were used to detect damage. This decision reflected the desire to use as few sensors as possible on a flexible space structure. Also, the FRFs from 0 to 60 Hz only were used in damage detection, because no modes above 60 Hz were included in model updating. An example of modeled and experimental FRFs for one of the damage cases is shown in Figure 22. Damage detection seemed promising based on the good fit between modeled and experimental data in this damage case. Notice that although the FRFs in Figure 22 were from collocated sensor-actuator pairs, they did not have the resonant-antiresonant interlacing pattern. This was because the damaged FTE was no longer symmetric; therefore, since multiple excitation was used, the FRFs obtained do not follow the collocated input-output FRF patterns. Each damaged FRF must be considered a multi-input single-output (MISO) FRF instead of a single-input single-output (SISO) FRF as in the undamaged case.

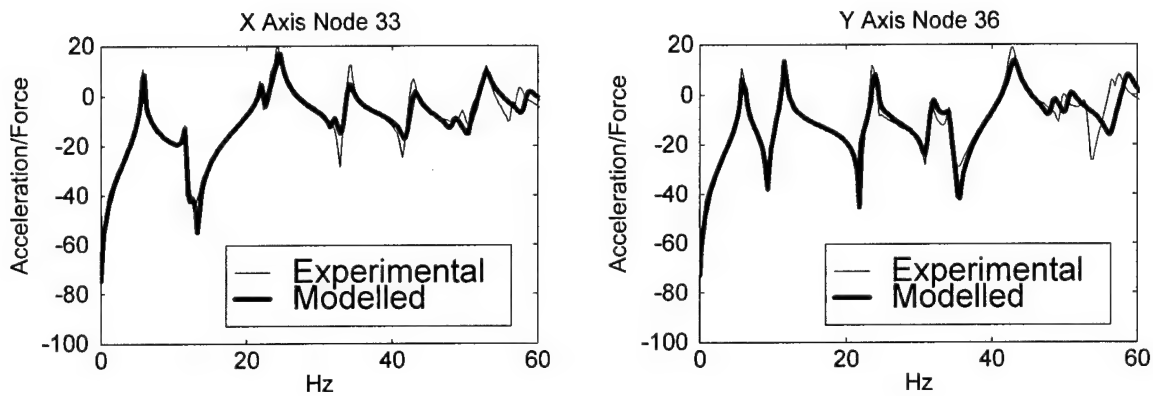

Figure 22. Member 17 Damaged FRFs

7.3 Pattern Classification Method

Swenson [37] developed a damage detection method that used pattern classifiers. The process reduces the experimental and modeled FRFs into feature vectors that contain the FRFs' characteristic properties. The feature extraction process is accomplished by integrating the area under the FRF curve using 40 weighted triangular filters spaced along the frequency axis. (Swenson used 20 triangular filters. Gaeta [11] achieved better damage detection results with 40 triangular filters.) The extracted features are arranged in a vector, which is then transformed via a discrete cosine transformation and plotted as a point in 40 dimensional space. One hundred training FRFs undergo this process so that a region in 40 dimensional space is defined by a statistical distribution of the 100 scattered points. The type of statistical methods used to describe this region defines the type of pattern classifier used. The Gaussian grand full pattern classifier used by Swenson was also used in this research.

Swenson's method of producing training data from the updated FE model was followed. Variability was added to the modeled FRFs to simulate the variability in the experimental data. The variability of the experimental data was measured by taking 100 experimental FRFs of the undamaged FTE. The mean FRF and the standard deviation of points away from the mean FRF was calculated. Using the MATLAB^{TM} random number generator, 100 training FRFs

were created that had the same standard deviation of points away from the modeled FRF as the experimental data had from the mean FRF. In order to ensure that the undamaged case was always correctly identified, 100 experimental FRFs were used for the undamaged training data. The undamaged FRFs were assumed to be known, since they were used in model updating.

The production of FE model training data assumed that the variability in the experimental FRF was independent of frequency, when in fact the experimental FRFs were especially noisy around resonances and antiresonances. This frequency dependent local variability in the experimental data was effectively spread over all frequencies in the modeled training data. This method also applied a variability derived from the undamaged FTE FRFs to the modeled training FRFs for damaged configurations. However, the variability of the damaged configuration FRFs may not have been the same as the undamaged variability. Despite these problems, this method was used to create training data for the pattern classifier.

Damage detection was accomplished by measuring the FRFs from the damaged FTE, extracting their features, and plotting the transformed feature vector, called the *test vector*, in 40 dimensional space. A discriminant function was computed from the test vector to each region representing the different damage cases. The discriminant function was based on the distances from the test vector to the damage case regions and on the statistical distributions (spread) of those regions. The region corresponding to the lowest discriminant function was identified as the actual damage case. For more details on damage detection using pattern classification, see Swenson [37].

7.4 Curve-Fit Method

The curve-fit method is a simple method of damage detection developed as part of this research. The method simply compared two test FRFs (x33 and y36) from the FTE to a catalog of FE FRFs of the different damage cases to see how well the curves fit. In order to ensure that the undamaged case was always correctly identified, experimental FRFs were used in the catalog for the undamaged case. The undamaged FRFs were assumed to be known, since they were used in

model updating. A cost function was computed as the sum of squared error between the two test FRFs and the two modeled FRFs. A cost was evaluated between the test FRFs and each of the damaged case FRFs in the catalog. The cost function used was:

$$J = \sum \left(\log \left| \left[\ \{H_{x33}\} \quad \{H_{y36}\} \ \right]_{Test} \right| - \log \left| \left[\ \{H_{x33}\} \quad \{H_{y36}\} \ \right]_{Model} \right| \right)^2 \qquad (57)$$

where H is a complex valued FRF vector.

The damage case corresponding to the lowest cost function was identified as the actual damage case.

7.5 Damage Detection Results - 32 Damage Cases

The first damage set consisted of 32 100% damaged diagonal configurations and one undamaged configuration. Both damage detection methods were tested against 3,300 test sets of x33 and y36 FRFs (100 for each of the 33 FTE configurations). The damage detection accuracy percentage of the pattern classifier and curve-fit methods are shown in Table 8. Swenson's damage detection results using the stiff model are included for comparison.

Table 8. Damage Detection Accuracy Rates (32 Damage Cases)

Updated FE Model	Damage Detection Method	Accuracy Rate (%)
Joint Model	Curve-Fit	100.0
Joint Model	Pattern Classifer	98.5
Stiff Model [37:56]	Pattern Classifier	79.0

Two comparisons can be made based on the results in Table 8. First, a comparison can be made between the joint model and the stiff model, since they were both used with pattern classifiers. The pattern classifier was much more accurate when using training data from the antiresonant updated joint model than when using the FRF updated stiff model. The second comparison that can be made is between the performance of the curve-fit and pattern classifier methods, since they both used the same FE model to detect damage. The curve-fit method was slightly more accurate than the pattern classifier, and it required only 0.6 seconds to identify damage compared to 3.5 seconds for the pattern classifier on a 166 MHz Pentium PC.

7.6 Damage Detection Results - 112 Damage Cases

A second damage set consisting of 112 damage configurations was also tested. This damage set included the 32 100% damage cases, 32 50% damaged diagonal cases, and 48 double damage cases. Both damage detection methods were tested against 11,300 test sets of x33 and y36 FRFs (100 for each of the 113 FTE configurations). The damage detection accuracy percentage of the pattern classifier and curve-fit methods are shown in Table 9. A breakdown of the types of errors made by the two types of damage detection method is included in Table 10.

Table 9. Damage Detection Accuracy Rates (113 Damage Cases)

Updated FE Model	Damage Detection Method	Accuracy Rate (%)
Joint Model	Curve-Fit	92.6
Joint Model	Pattern Classifer	76.1

Table 10. Damage Detection Accuracy Breakdown

Damage Category	Curve-Fit Method $\left(\frac{\text{Cases Always Correctly Identified}}{\text{Number of Possible Cases}}\right)$	Pattern Classifier Method $\left(\frac{\text{Cases Always Correctly Identified}}{\text{Number of Possible Cases}}\right)$
Undamaged	$\frac{1}{1}$	$\frac{1}{1}$
50% Damaged	$\frac{16}{32}$	$\frac{2}{32}$
100% Damaged	$\frac{32}{32}$	$\frac{31}{32}$
Double Damaged	$\frac{48}{48}$	$\frac{45}{48}$

Again, the curve-fit method was more accurate than the pattern classifier. The errors made by the curve-fit method were all confined to 50% damaged members. This indicated that the FRFs of the undamaged FTE and the 50% damaged diagonal cases were all very similar. The slight experimental FRF changes due to damage were small enough to be indistinguishable from the initial mismatch between model and experimental FRFs caused by errors in the FE model. Lastly,

it was observed that the curve-fit method required 0.7 seconds to identify damage from a test set of FRFs compared to 3.6 seconds for the pattern classifier on a 166 MHz Pentium PC.

The fact that the curve-fit method was 100% successful in identifying all 100% damage and double damage cases, using only two sensors, validated the physical correctness of the antiresonant updated joint model. The high quality of the joint model was attributed to the use of rigid links that were updated using antiresonances. Furthermore, it was found that the curve-fit method was a better damage detection method than the pattern classifier method based on the fact that it produced more accurate results, required less computation, and did not require training data.

The damage detection results in this research could be improved upon by using the natural frequencies and antiresonant frequencies of an FRF as characteristic features, because they (assuming light damping) completely define the FRF (see equation (3)). A frequency change vector could be defined as the damaged natural frequencies and antiresonant natural frequencies minus their undamaged values. To first order, this would remove the model errors from the damage detection process, since the errors are present in both the modeled undamaged FRF and the modeled damaged FRF [10]. This method would require an automatic identification tool that would quickly extract the natural frequencies and antiresonant natural frequencies, which may be complex, from an FRF. The tool must extract specific natural frequencies and antiresonances so that they correlate with the identified undamaged natural frequencies and antiresonances. The development of an automatic antiresonance identification tool is a recommended area for further research.

Chapter 8 - Conclusions and Recommendations

This research made contributions in the areas of modeling the FTE, FE model updating, and damage detection. The results from these areas will be briefly reviewed. Conclusions and recommendations from this research follow at the end of the chapter.

8.1 Joint Modeling Results

A new FE model of the FTE was created based on the conclusions of previous researchers that the majority of the error in previous models was due to inaccurate modeling of the joints. The model created for this research, called the joint model, was designed to improve the modeling of the FTE joints. The approach taken was to parameterize the joints with rigid links of variable lengths. During updating, the rigid link dimensions changed, stiffening the joints as they grew and softening the joints as they shrunk. The lumped masses of the diagonal ends were lumped in their physically accurate locations via another rigid link, which was held constant. This model was the first to produce the correct resonance-antiresonance order in all of the FTE FRFs even before updating. Two critical elements to producing this correct order was the modeling of the regular batten joints with rigid links and the elimination of the proof mass actuator mass in the direction of actuation. Even with these modeling improvements the joint model had only 192 DOF.

8.2 Finite Element Model Updating Using Antiresonance Results

The iterative modal update method, called the penalty method, was expanded to include antiresonant frequencies. This method proved especially versatile in that it allowed antiresonance data, the use of virtually any parameter in the model as an update parameter, and the use of measurement and parameter weights. The penalty method was also very efficient because it used sensitivities to determine steps in the update parameters. The parameters chosen for the FTE were five joint rigid link dimensions along with two beam properties. The antiresonant update was highly successful in that it was fast (approximately 20 minutes on a 166 MHz Pentium PC),

produced parameter changes of reasonable size, and produced a model that matched experimental data well. The antiresonant updated model produced FRFs that had a 46% better correlation to experimental FRFs than the same model updated using only natural frequencies.

8.3 Damage Detection Results

Damage detection was used as a test of the physical correctness of the antiresonant updated joint model. The updated model was used to predict the FRFs of the FTE in damaged configurations. The modeled damage FRFs were used with two different damage detection methods. The first method, called the pattern classifier method, condensed the modeled FRFs into feature vectors which were plotted in 40 dimensional space. Test FRFs were then taken from the FTE, condensed into feature vectors and plotted in 40 dimensional space. The method determined the damage case as the "nearest region" (in some statistical sense) to the test vector. The second method, developed as part of this research and called the curve-fit method, took the modeled FRFs and assembled them into a catalog of possible damage cases. Test FRFs were then taken from the FTE. A cost function was computed as the sum of squared error between the test FRFs and each modeled FRF in the catalog of possible damage cases. The damage was identified as the damage case with the lowest cost function.

Damage to the FTE was simulated in three ways. In the first method, called 100% damage cases, one diagonal was removed from the FTE. In the second method, called the 50% damage cases, one diagonal was replaced with a diagonal of only 50% the normal cross sectional area. In the third method, called the double damage cases, two diagonals were simultaneously removed from a single bay of the FTE. These damage cases were modeled by removing the appropriate elements or replacing them with elements of 50% normal cross sectional area in the joint model.

The first damage detection test considered only the 32 100% damaged diagonal cases. The accuracy rates for the two damage detection methods in identifying the 32 damage cases are shown in Table 11. The second damage detection test considered 112 damage cases consisting of the

32 100% damaged cases, 32 50% damaged cases, and 48 double damaged cases. The accuracy rates for damage detection with 112 cases is shown in Table 12. The curve-fit method produced better accuracy rates in both tests, which raises a question about the benefits of using the more complicated pattern classifier method.

Table 11. Damage Detection Accuracy Rates (32 Damage Cases)

Damage Detection Method	Accuracy Rate (%)
Curve-Fit	100.0
Pattern Classifer	98.5

Table 12. Damage Detection Accuracy Rates (113 Damage Cases)

Damage Detection Method	Accuracy Rate (%)
Curve-Fit	92.6
Pattern Classifer	76.1

The breakdown in Table 13 shows where the errors in damage detection occurred. The fact that the curve-fit method was 100% successful in identifying all 100% damage and double damage cases, using only two sensors, validated the physical correctness of the antiresonant updated joint model. The 50% damage FRFs were too similar to each other and to the undamaged FRFs to reliably predict the damaged member.

Table 13. Damage Detection Accuracy Breakdown

Damage Category	Curve-Fit Method $\left(\frac{\text{Cases Always Correctly Identified}}{\text{Number of Possible Cases}}\right)$	Pattern Classifier Method $\left(\frac{\text{Cases Always Correctly Identified}}{\text{Number of Possible Cases}}\right)$
Undamaged	$\frac{1}{1}$	$\frac{1}{1}$
50% Damaged	$\frac{16}{32}$	$\frac{2}{32}$
100% Damaged	$\frac{32}{32}$	$\frac{31}{32}$
Double Damaged	$\frac{48}{48}$	$\frac{45}{48}$

8.4 Conclusions and Recommendations

Several conclusions can be made based on this research. In the area of joint modeling, rigid links were an effective and simple joint modeling method. The rigid links were also convenient update parameters for FE model updating. The updated joint model proved to be an excellent model of the FTE in both undamaged and damaged configurations. The updated joint model should be used in further FTE related research projects focusing on model updating, damage detection, vibration control, or other topics.

In the area of FE model updating, antiresonant frequencies improved the stability of model updating and produced a more accurate model than updating with natural frequencies only. The fact that the antiresonant updated model produced excellent models of damaged configurations of the structure indicated that antiresonance updating corrected modeling errors and produced a physically accurate model. Antiresonance updating should be applied in further experimental studies and compared with other FE model update methods, especially those that include mode shape data.

In the area of damage detection, the simple sum-of-squared error cost function used in the curve-fit method was more accurate in detecting damage than the pattern classifier. Both the cost function and pattern classifier were unable to reliably locate a 50% damaged member in the structure. FRF damage detection methods, such as the cost function and pattern classifier, are unable to differentiate whether the mismatch between modeled and experimental data is due to slight damage or FE model errors. Therefore, methods that use the changes in natural frequencies and antiresonant frequencies from undamaged values, should be preferred over FRF based damage detection methods. Frequency change methods should be more accurate because they remove the FE model error to first order from the damage detection process [10]. Frequency change methods were not attempted in this research, because a reliable automatic antiresonant identification tool was not found. Research should also be conducted on the development of an automatic

antiresonance identification tool for model updating and damage detection, which will identify the antiresonant frequencies from experimental FRFs.

Damage detection research on the FTE should be expanded so that a catalog of pre-defined possible damage cases is not required. The concepts of model updating can be used so that update parameters converge to values that identify damage location and severity. This is a difficult and ill-defined problem, since there will be many possible parameters necessary to describe any arbitrary damage. Antiresonance data can improve the conditioning of the damage detection problem by increasing the amount and accuracy of measured information available. Antiresonance shows great promise in improving FE model updating and damage detection methods.

APPENDIX A - Flexible Truss Experiment Member Properties

This appendix gives the element mass and stiffness matrices and the material and geometric properties of the FTE's members. Material and geometric properties of the FTE's members are taken from Swenson [37] with some slight modifications. Exact dimensions of the FTE can be found in Swenson [37].

A.1 Element Matrices

For the 12 DOF beam element the element mass and stiffness matrices are:

$$[m] = \begin{bmatrix} [m_1] & [m_2] \\ [m_3] & [m_4] \end{bmatrix}$$

$$[m_1] = \frac{\rho AL}{420} \begin{bmatrix} 140 & 0 & 0 & 0 & 0 & 0 \\ 0 & 156 & 0 & 0 & 0 & 22L \\ 0 & 0 & 156 & 0 & -22L & 0 \\ 0 & 0 & 0 & 140J & 0 & 0 \\ 0 & 0 & -22L & 0 & 4L^2 & 0 \\ 0 & 22L & 0 & 0 & 0 & 4L^2 \end{bmatrix}$$

$$[m_2] = \frac{\rho AL}{420} \begin{bmatrix} 70 & 0 & 0 & 0 & 0 & 0 \\ 0 & 54 & 0 & 0 & 0 & -13L \\ 0 & 0 & 54 & 0 & 13L & 0 \\ 0 & 0 & 0 & 70J & 0 & 0 \\ 0 & 0 & -13L & 0 & -3L^2 & 0 \\ 0 & 13L & 0 & 0 & 0 & -3L^2 \end{bmatrix}$$

$$[m_3] = \frac{\rho AL}{420} \begin{bmatrix} 70 & 0 & 0 & 0 & 0 & 0 \\ 0 & 54 & 0 & 0 & 0 & 13L \\ 0 & 0 & 54 & 0 & -13L & 0 \\ 0 & 0 & 0 & 70J & 0 & 0 \\ 0 & 0 & -13L & 0 & -3L^2 & 0 \\ 0 & -13L & 0 & 0 & 0 & -3L^2 \end{bmatrix}$$

$$[m_4] = \frac{\rho AL}{420} \begin{bmatrix} 140 & 0 & 0 & 0 & 0 & 0 \\ 0 & 156 & 0 & 0 & 0 & -22L \\ 0 & 0 & 156 & 0 & 22L & 0 \\ 0 & 0 & 0 & 140J & 0 & 0 \\ 0 & 0 & 22L & 0 & 4L^2 & 0 \\ 0 & -22L & 0 & 0 & 0 & 4L^2 \end{bmatrix}$$

$$[k] = \begin{bmatrix} [k_1] & [k_2] \\ [k_3] & [k_4] \end{bmatrix}$$

$$[k_1] = \frac{E}{L^3} \begin{bmatrix} AL^2 & 0 & 0 & 0 & 0 & 0 \\ 0 & 12I & 0 & 0 & 0 & 6IL \\ 0 & 0 & 12I & 0 & -6IL & 0 \\ 0 & 0 & 0 & \frac{GJL^2}{E} & 0 & 0 \\ 0 & 0 & -6IL & 0 & 4L^2 & 0 \\ 0 & 6IL & 0 & 0 & 0 & 4L^2 \end{bmatrix}$$

$$[k_2] = \frac{E}{L^3} \begin{bmatrix} -AL^2 & 0 & 0 & 0 & 0 & 0 \\ 0 & -12I & 0 & 0 & 0 & 6IL \\ 0 & 0 & -12I & 0 & -6IL & 0 \\ 0 & 0 & 0 & -\frac{GJL^2}{E} & 0 & 0 \\ 0 & 0 & 6IL & 0 & 2L^2 & 0 \\ 0 & -6IL & 0 & 0 & 0 & 2L^2 \end{bmatrix}$$

$$[k_3] = \frac{E}{L^3} \begin{bmatrix} -AL^2 & 0 & 0 & 0 & 0 & 0 \\ 0 & -12I & 0 & 0 & 0 & -6IL \\ 0 & 0 & -12I & 0 & 6IL & 0 \\ 0 & 0 & 0 & -\frac{GJL^2}{E} & 0 & 0 \\ 0 & 0 & -6IL & 0 & 2L^2 & 0 \\ 0 & 6IL & 0 & 0 & 0 & 2L^2 \end{bmatrix}$$

$$[k_4] = \frac{E}{L^3} \begin{bmatrix} AL^2 & 0 & 0 & 0 & 0 & 0 \\ 0 & 12I & 0 & 0 & 0 & -6IL \\ 0 & 0 & 12I & 0 & 6IL & 0 \\ 0 & 0 & 0 & \frac{GJL^2}{E} & 0 & 0 \\ 0 & 0 & 6IL & 0 & 4L^2 & 0 \\ 0 & -6IL & 0 & 0 & 0 & 4L^2 \end{bmatrix}$$

$$\{d\} = \begin{bmatrix} u_1 & v_1 & w_1 & \gamma_1 & \theta_1 & \xi_1 & u_2 & v_2 & w_2 & \gamma_2 & \theta_2 & \xi_2 \end{bmatrix}^T$$

where

$\{d\}$ = nodal displacement DOF as shown in Figure 10

ρ = mass density (lb_m/in^3)

L = the length of the beam (in)

J = the polar moment of inertia of the cross sectional area (in^4)

E = Young's modulus of elasticity (lb_f/in^2)

G = shear modulus of elasticity (lb_f/in^2)

A = the cross sectional area (in^2)

I = the moment of inertia of the cross sectional area (in^4)

A.2 Material Properties

Aluminum Properties	
Mass density(ρ)	2.699 g/cm^{3}or 2.54E-4 lb_m/in^3
Modulus of elasticity (E)	9.9E+6 lb_f/in^2
Modulus of elasticity in shear (G)	3.8E+6 lb_f/in^2

Table 14. Aluminum Properties [37]

Lexan Properties	
Mass density(ρ)	.99 g/cm^3 or 9.32E-5 lb_m/in^3
Modulus of elasticity (E)	5.01E+5 lb_f/in^2
Modulus of elasticity in shear (G)	1.5E+5 lb_f/in^2

Table 15. Lexan Properties [37]

A.3 Geometric Properties

A.3.1 Longerons

$$L = 29.44 \text{ in}$$

$$A = 0.3731 \text{ in}^2$$

$$I_y = I_x = 0.12831 \text{ in}^4$$

$$J = 0.25662 \text{ in}^4$$

A.3.2 Regular and Top Battens

$$
\begin{aligned}
L &= 18.375 \text{ in} \\
A &= 0.11012 \text{ in}^2 \\
I_y &= I_x = 3.5779 \times 10^{-3} \text{ in}^4 \\
J &= 7.1558 \times 10^{-3} \text{ in}^4
\end{aligned}
$$

A.3.3 Mid Battens

$$
\begin{aligned}
L &= 18.375 \text{ in} \\
A &= 0.22025 \text{ in}^2 \\
I_y &= 7.1558 \times 10^{-3} \text{ in}^4 \\
I_x &= 0.0622 \text{ in}^4 \\
J &= 0.06937 \text{ in}^4
\end{aligned}
$$

A.3.4 Diagonals

$$
\begin{aligned}
L &= 34.33 \text{ in} \\
A &= 0.54 \text{ in}^2 \\
I_y &= I_x = 0.12866 \text{ in}^4 \\
J &= 0.25732 \text{ in}^4
\end{aligned}
$$

A.3.5 50% Damaged Diagonal

$$L = 34.33 \text{ in}$$

$$A = 0.27 \text{ in}^2$$

$$I_y = 0.018 \text{ in}^4$$

$$I_x = 0.06433 \text{ in}^4$$

$$J = 0.0823 \text{ in}^4$$

Bibliography

[1] Afolabi, D. "An Anti-Resonance Technique for Detecting Structural Damage," *Proceedings of the 5th International Modal Analysis Conference*, pages 491-495, 1987.

[2] Ahmadian, H., J. Mottershead and M. Friswell. "Joint Modelling for Finite Element Model Updating," *Proceedings of the 14th International Modal Analysis Conference*, pages 591-596, 1996.

[3] Balmes, Etienne. *Structural Dynamics Toolbox User Manual*. Scientific Software Group, 1997.

[4] Belvin, Keith W. Modeling of Joints for the Dynamic Analysis of Truss Structures. NASA Technical Paper 2661, May 1987.

[5] Cobb, Richard G. *Structural Damage Identification From Limited Measurement Data*. PhD dissertation, Air Force Institute of Technology (AU), Wright-Patterson AFB OH, March 1996.

[6] Cook, Robert D. and others. *Concepts and Applications of Finite Element Analysis*. New York: John Wiley & Sons, Inc., 1989.

[7] Doebling, S., C. Farrar, M. Prime, and D. Shevitz. *Damage Identification and Health Monitoring of Structural and Mechanical System from Changes in their Vibration Characteristics: A Literature Review*. Las Alamos National Laboratory Report LA-13070-MS. http://lib-www.lanl.gov/la-pubs/00285981.pdf. May 1996.

[8] Feng-Quan, Wang, Han Xia-Ling and Guo Ying-Zheng. "Analysis of the Characteristics of Pseudo-Resonance and Anti-Resonance," *Journal of Vibration and Acoustic*, vol. 118, pages 663-667, October 1996.

[9] Friswell, M. I. and J. E. Mottershead. *Finite Element Model Updating and Structural Dynamics*. Kluwer: Academic Press, 1995.

[10] Friswell, M. I. and J. E. T. Penny. "Is Damage Location Using Vibration Measurements Practical?" *EUROMECH 365 International Workshop: DAMAS 97, Structural Damage using Advanced Signal Processing Procedures, Sheffield, UK, June/July 97*, http://www.swan.ac.uk/mecheng/staff/mfriswell/PDF_Files/DAMAS97.html.

[11] Gaeta, Douglas. *Damage Identification in a Real Structure Using Resonant and Antiresonant Frequencies*. MS thesis, AFIT/GA/ENY/00-02. Air Force Institute of Technology (AU), Wright-Patterson AFB OH, March 2000.

[12] Gordon, Robert W. *The 12-Meter Truss Active Control Experiment Design, Analysis, and Open-Loop Testing*. Technical Report WL-TR-92-3012, Flight Dynamics Directorate, Wright Laboratory, Air Force Systems Command, Wright-Patterson AFB, OH, 1992.

[13] Harris, Cyril M. *Shock and Vibration Handbook*. New York: McGraw Hill, 3rd ed., 1988.

[14] He, J. and Y.-Q. Li. "Relocation of Anti-Resonances of a Vibratory System by Local Structural Changes," *The International Journal of Analytical and Experimental Modal Analysis*, v10(4), pages 224-235, Oct 1995.

[15] Horton, B., H. Gurgenci, M. Veidt, and M.I. Friswell. "Finite Element Model Updating of the Welded Joints in a Tubular H-Frame." *Proceedings of the 17th International Modal Analysis Conference*, pages 1556-1562, 1999.

[16] Inman, Daniel J. *Vibration with Control, Measurement, and Stability*. New Jersey: Prentice Hall, 1990.

[17] Kienholtz, David A. *Scaling of Large Space Structural Joints*. AFWAL-TR-88-3047, AD-A197 027, Flight Dynamics Laboratory, Wright Patterson AFB OH, 1988.

[18] La Civita, M. and A. Sestieri. "On Antiresonance Interpretation and Energy Concentration Along Continuous One-Dimensional Systems," *Proceedings of the 15th International Modal Analysis Conference*, pages 778-784, 1997.

[19] Lallement, G. and S. Cogan. "Reconciliation Between Measured and Calculated Dynamic Behaviors : Enlargement of the Knowledge Space," *Proceedings of the 10th International Modal Analysis Conference*, pages 487-493, 1992.

[20] Mathworks Inc. *Using Matlab Version 5*. 1996.

[21] Meirovitch, Leonard. *Elements of Vibration Analysis*. Boston: McGraw Hill, 1986.

[22] Moore, Gregory J. *MSC/NASTRAN Design Sensitivity and Optimization User's Manual*. 1994.

[23] Mottershead, J. E. and M. I. Friswell. "Model Updating in Structural Dynamics: A Survey," *Journal of Sound and Vibration*, 167(2):347-375, 1993.

[24] Mottershead, J. E., M. I. Friswell, G. H. T. Ng, and J. A. Brandon. "Geometric Parameters for Finite Element Model Updating of Joints and Constraints," *Mechanical Systems and Signal Processing*, 10(2), pages 171-182, 1996.

[25] Mottershead, J. E. and M. I. Friswell. "Editorial," *Mechanical Systems and Signal Processing*, 12(1):1-6, 1998.

[26] Mottershead, John E. "On the Zeros of Structural Frequency Response Functions and their Application to Model Assessment and Updating," *Proceedings of the 16th International Modal Analysis Conference*, pages 500-503, 1998.

[27] Mottershead, J. E. "On the Natural Frequencies and Antiresonances of Modified Structures," *Proceedings of the 17th International Modal Analysis Conference*, pages 648-653, 1999.

[28] Peyt, Maurice. *Introduction to Finite Element Analysis*. New York: Cambridge University Press, 1990.

[29] Prabhu, Annappa A. "Use of Finite Element Analysis to Study the Effect of Joints and Stress on Damping in Space Flight Hardware," Paper- AIAA 93-1488 presented at the 34th

AIAA/ASME/ASCE/AHS/ASC Structures, Structural Dynamics and Materials Conference, Adaptive Structures Forum, April 1993.

[30] Rade, Domingos A., Gerard Lallement, and Leandro Afonso da Silva. "A Strategy for the Enrichment of Experimental Data as Applied to an Inverse Eigensensitivity-Based F.E. Model Updating Method," *Proceedings of the 14th International Modal Analysis Conference*, pages 1078-1085, 1996.

[31] Reid, Gary J. *Linear System Fundamentals - Continuous and Discrete, Classic and Modern*. New York: McGraw Hill, Inc., 1983.

[32] Reymond, Michael and Mark Miller. *MSC/NASTRAN Quick Reference Guide*. The MacNeal-Schwendler Co. 1994.

[33] Rogers, Lynn C. "Derivatives of Eigenvalues and Eigenvectors," *AIAA Journal*, Vol. 8, pages 943-944, May 1970.

[34] Schrader, Cheryl B., and Michael K. Sain. "Research on System Zeros: a Survey," *International Journal of Control*, vol. 50 no. 4, pages 1407-1433, 1989.

[35] Scientific Atlanta Inc. *SA390 Operators Manual*. March 1996.

[36] Suarez, Luis E. and Enrique E. Matheu. *The Flexibility Effects on the Dynamic Response of Structures - Part I: Deterministic Analysis*. Final Report, US Army Research Office, DTIC AD-A260 487, December 1992.

[37] Swenson, Eric D. *Damage Detection Using Pattern Classifiers*. MS thesis, AFIT/GA/ENY/98-01. Air Force Institute of Technology (AU), Wright-Patterson AFB OH, March 1998.

[38] Tohyama, Mikio and Richard H. Lyon. "Zeros of a Transfer Function in a Multi-Degree-of-Freedom Vibrating System," *Journal of the Acoustical Society of America*, 86(5), pages 1854-1863, November 1989.

[39] Tsai, J. S. and Y. F. Chou. "The Identification of Dynamic Characteristics of a Single Bolt Joint," *Journal of Sound and Vibration*, 125(3), pages 487-502, 1988.

[40] Wahl, F., G. Schmidt, and L. Forrai. "On the Significance of Antiresonance Frequencies in Experimental Structural Analysis," *Journal of Sound and Vibration*, 219(3), pages 379-394, 1999.

[41] Wang, Bo Ping. "Antiresonance and its Sensitivity Analysis in Structural Systems," Papers- AIAA-98-1751, pages 431-440, 1998.

[42] Wang, J. and P. Sas. "A Method for Identifying Parameters of Mechanical Joints," *Journal of Applied Mechanics*, Vol.57, pages 337-342, June 1990.

[43] Williams, Trevor and Jer-Nan Juang. "Sensitivity of the Transmission Zeros of Flexible Space Structures," *Journal of Guidance, Control, and Dynamics*, Vol. 15, No. 2, March-April 1992.

[44] Zill, Dennis G. and Michael R. Cullen. *Advanced Engineering Mathematics*. Boston: PWS-Kent Publishing, 1992.

Vita

Keith W. Jones was born on February 5, 1974 in Fairfield, CA. In 1991, Keith accepted Jesus as his Lord and Savior and was baptized in Vista Grande Baptist Church of Colorado Springs, CO. In June of 1992, he graduated from Doherty High School in Colorado Springs and entered the United States Air Force Academy (USAFA). Four years later he was commissioned after graduating with academic distinction and a degree in Mechanical Engineering. After marrying Ms. Claudia DaCruz of Colorado Springs, Second Lieutenant Jones went to Edwards AFB, CA where he served two years as a mechanical subsystems engineer in the 418th Flight Test Squadron. His responsibilities included project management as well as test planning, conducting, and reporting on various C-130, C-141, and C-17 flight test projects. In 1998, First Lieutenant Jones was selected to attend the Air Force Institute of Technology to earn a Masters of Science in Aeronautical Engineering. After graduation, Lieutenant Jones will be working for the Propulsion Directorate, Air Force Research Laboratory, Wright-Patterson Air Force Base, Ohio.

Permanent Address: 3202 Red Onion Circle

Colorado Springs, CO 80918

REPORT DOCUMENTATION PAGE

Form Approved
OMB No. 0704-0188

Public reporting burden for this collection of information is estimated to average 1 hour per response, including the time for reviewing instructions, searching existing data sources, gathering and maintaining the data needed, and completing and reviewing the collection of information. Send comments regarding this burden estimate or any other aspect of this collection of information, including suggestions for reducing this burden, to Washington Headquarters Services, Directorate for Information Operations and Reports, 1215 Jefferson Davis Highway, Suite 1204, Arlington, VA 22202-4302, and to the Office of Management and Budget, Paperwork Reduction Project (0704-0188), Washington, DC 20503.

1. AGENCY USE ONLY *(Leave blank)*

2. REPORT DATE
March 2000

3. REPORT TYPE AND DATES COVERED
Master's Thesis

4. TITLE AND SUBTITLE
FINITE ELEMENT MODEL UPDATING USING ANTIRESONANT FREQUENCIES

5. FUNDING NUMBERS

6. AUTHOR(S)
Keith W. Jones, 1Lt., USAF

7. PERFORMING ORGANIZATION NAME(S) AND ADDRESS(ES)
Air Force Institute of Technology
Graduate School of Engineering and Management (AFIT/EN)
2950 P. Street, Building 640
WPAFB OH 45433-7765

8. PERFORMING ORGANIZATION REPORT NUMBER
AFIT/GAE/ENY/00M-08

9. SPONSORING/MONITORING AGENCY NAME(S) AND ADDRESS(ES)
AFRL/VSDV
3550 Aberdeen Ave. SE
Kirtland AFB, NM 87117-5776

10. SPONSORING/MONITORING AGENCY REPORT NUMBER

11. SUPPLEMENTARY NOTES
Advisor: LtCol Jeffrey Turcotte, ENY, DSN: 785-3636, ext. 4597

12a. DISTRIBUTION AVAILABILITY STATEMENT
APPROVED FOR PUBLIC RELEASE; DISTRIBUTION UNLIMITED.

12b. DISTRIBUTION CODE

13. ABSTRACT *(Maximum 200 words)*

The applications of antiresonant frequencies to finite element (FE) model updating are few and usually limited to numerical examples. This work uses antiresonant frequencies in the model updating of an experimental structure and analyzes the physical correctness of the updated model by using it to detect damage.

Antiresonant frequencies were used in the model updating of a six-meter aluminum truss. The model used rigid links to model welded and bolted joints. Rigid link dimensions were used as update parameters in an iterative update based on eigenvalues and antiresonance sensitivities. The first update used 11 natural frequencies and 21 antiresonant frequencies from seven experimental frequency response functions (FRFs). The second update used only 11 natural frequencies. The antiresonant updated model produced a 46% better correlation to experimental FRFs than the non-antiresonant updated model.

The antiresonant updated model was used to predict FRFs for the FTE in 112 damaged configurations. Pattern classification and curve-fit algorithms for damage detection were tested. The curve-fit method correctly identified damage 92.6% of the time compared to 76.1% for the pattern classifier. The high quality of the model was attributed to the use of rigid links that were updated using antiresonant frequencies.

14. SUBJECT TERMS
Finite Element Analysis, Damage, Detection, Joints
Finite Element Model Updating, Antiresonant Frequencies, Antiresonance, Pattern Classifier

15. NUMBER OF PAGES
94

16. PRICE CODE

17. SECURITY CLASSIFICATION OF REPORT	18. SECURITY CLASSIFICATION OF THIS PAGE	19. SECURITY CLASSIFICATION OF ABSTRACT	20. LIMITATION OF ABSTRACT
UNCLASSIFIED	UNCLASSIFIED	UNCLASSIFIED	UL